An In Situ Infrared Spectroscopic Investigation of the Rh-Catalyzed [5+1+2+1] Cycloaddition Reaction of Vinylcyclopropanes, Terminal Alkynes, and Carbon Monoxide

By
Ryan Nelson McCoy

A Thesis Submitted to
Saint Mary's University, Halifax, Nova Scotia
in Partial Fulfillment of the Requirements for
the Degree of Bachelor of Science
with Honours in Chemistry

April 2019, Halifax, Nova Scotia

Approved: Dr. Kai Ylijoki
Supervisor
Department of Chemistry

Approved: Dr. Jason Masuda
Chairperson
Department of Chemistry

Date: April 18, 2019

An In Situ Infrared Spectroscopic Investigation of the Rh-Catalyzed [5+1+2+1] Cycloaddition Reaction of Vinylcyclopropanes, Terminal Alkynes, and Carbon Monoxide

By Ryan Nelson McCoy

Abstract

In the [5+1+2+1] cycloaddition reaction, hydroxydihydroindanones can be synthesized from vinylcyclopropanes and alkynes under a carbon monoxide atmosphere to produce five new C-C bonds in a single step. Dihydroindanones are typically produced through reduction of indenones. However, since various multistep methods are used to obtain indenones, the single step [5+1+2+1] cycloaddition reaction provides an attractive, alternative synthetic route. The vinylcyclopropane (VCP) starting material has been successfully prepared through modification of a previously reported 3-step synthetic method. The [5+1+2+1] cycloaddition reaction reported by Wender et al. was tested and confirmed to work with the synthesized VCP, as crystals of the desired hydroxydihydroindanone cycloaddition product were obtained.

In situ infrared spectroscopic studies of the cycloaddition reaction were performed. Although these studies were unsuccessful in identifying reaction intermediates of the cycloaddition pathway, second derivative analysis of the spectroscopic data successfully resolved overlapping CO peaks. The experimentally obtained spectra of the reaction solution could not be compared to theoretical pure spectra of components believed to be in solution, as the IR frequency calculations (performed using the functional and basis set needed to apply a reported vibrational scaling factor) failed to converge to a minimum. Finally, a DFT investigation of the monometallic and bimetallic cycloaddition pathways was performed. This investigation suggested that the bimetallic pathway is both kinetically and thermodynamically favourable, which is inconsistent with previous experimental results.

April 18, 2019

Acknowledgements

I would firstly like to thank Dr. Kai Ylijoki for being my thesis supervisor. He is an excellent mentor and teacher, and his ability to skillfully convey concepts has always impressed me. I also thank Ernlie Publicover of the Ylijoki group for being so patient with me and for helping me out with my experiments when I needed a second pair of hands.

I would additionally like to thank Dr. Jason Clyburne for letting me get my foot in the door into the world of research. One member of the Clyburne group I would especially like to thank is Dr. Kathy Robertson. Her sense of humour never fails to bring a smile to my face or make me laugh, and she has also given me important guidance during my time at SMU. She is a brilliant crystallographer who makes it look easy, and I deeply admire her intellect, patience, and strong work ethic.

I would like to thank my friends and family, who have always been there for me. Finally, I would like to thank Dr. Jon Kabat-Zinn for introducing me to mindfulness meditation with his books *Mindfulness for Beginners* and *Full Catastrophe Living*. These books have changed my perspective and have therefore changed my life.

"Oh, I've had my moments, and if I had to do it over again, I'd have more of them. In fact, I'd try to have nothing else. Just moments, one after another, instead of living so many years ahead of each day." – *Nadine Stair, 85 years old, Louisville, Kentucky*

Table of Contents

List of Figures

List of Schemes

List of Tables

Table of Symbols and Abbreviations

ν_{CO}	carbonyl stretching frequency
ΔG	Gibbs free energy
Å	Angstrom (10^{-10} m)
a priori	from Latin, meaning "from the earlier"
atm	atmosphere
ATR	attenuated total reflectance
B3LYP	Becke, three-parameter, Lee-Yang-Parr hybrid functional
br	broad
ca.	circa (from Latin, meaning "about, approximately")
$CDCl_3$	deuterated chloroform
cm^{-1}	wavenumber
CO	carbon monoxide
d	doublet
DFT	Density Functional Theory
Eqn.	equation
Equiv.	equivalent
et al.	et alii (from Latin, meaning "and others")
g	gram
HP-IR	high pressure infrared
HRMS	high-resolution mass spectrometry
HSQC	heteronuclear single quantum correlation
in situ	from Latin, meaning "on site, in position" (i.e., in the reaction mixture)
in vacuo	from Latin, meaning "in a vacuum"
INT	intermediate
IR	infrared
J	coupling constant
m	multiplet/medium
MHz	megahertz
mL	milliliter
mmol	millimole
NBS	N-bromosuccinimide
NMR	nuclear magnetic resonance
^oC	degrees Celsius
PCM	polarizable continuum model
PM3	parameterized model number 3, semi-empirical method
RDS	rate determining step
q	quartet
s	singlet/strong
t	triplet
TLC	thin layer chromatography

TMS	tetramethylsilane
Toluene-d_8	deuterated toluene
TRIR	time resolved infrared
TS	transition state
VCP	1-(2-methoxyethoxy)-1-vinylcyclopropane
vide infra	from Latin, meaning “see below, see further on”
vs	very strong
w	weak
λ	wavelength

Chapter 1 – Introduction

1.1 The [5+1+2+1] Cycloaddition Reaction

Cycloaddition reactions are a vital tool in the toolbox of the synthetic organic chemist. This class of reaction can be promoted by conditions such as heat, light, and Lewis acids. The presence of polarized functional groups in the substrate is often required in many of these reaction conditions in order for the reaction to proceed. Metal catalysts have provided new opportunities for cycloaddition chemistry, as the complexation of the metal center to a double or triple bond significantly changes the reactivity of the moiety.[1] Rhodium has found wide application as a catalyst in the field of cycloaddition chemistry, one such application being the rhodium catalyzed [5+1+2+1] cycloaddition reaction involving vinylcyclopropanes (VCPs), terminal alkynes, and carbon monoxide reported by Wender et al.[2] in 2005 (Scheme 1.1). The numbers in brackets refer to the number of carbons of each component (involved in ring formation), and the ordering of the numbers refers to the order of coordination (and subsequent insertion) of each component on the metal center. The [5+1+2+1] cycloaddition reaction has been recently investigated using DFT and NMR spectroscopy to elucidate the reaction mechanism.[3,4]

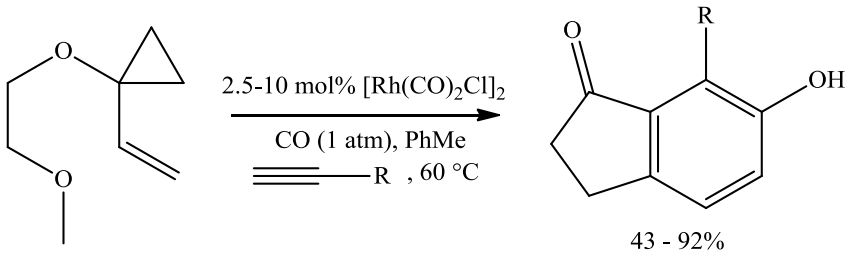

Scheme 1.1: The Rh-catalyzed [5+1+2+1] cycloaddition reaction of VCPs, terminal alkynes, and CO.[2]

In these NMR studies previously conducted (vide infra), higher catalyst loadings were used in an attempt to observe the reaction intermediates. These higher loadings led to the formation of a bimetallic species that prevented the reaction from proceeding. Since infrared spectroscopy is more sensitive than NMR spectroscopy, it was hypothesized that in situ IR may be a more suitable method for observing reaction intermediates, given that lower catalyst loadings need to be used for the reaction to proceed.

1.2 The Importance and Application of the [5+1+2+1] Cycloaddition Reaction

In the [5+1+2+1] cycloaddition reaction, hydroxydihydroindanones can be synthesized from vinylcyclopropanes and alkynes under a carbon monoxide atmosphere to produce five new C-C bonds in a single step.[2] Dihydroindanones are typically produced through reduction of indenones. However, since various multistep methods are used to obtain indenones, the single step [5+1+2+1] cycloaddition reaction provides an attractive, alternative synthetic route.[3]

With regard to application, indenone compounds have found use as novel cyclooxygenase-2 (COX-2) enzyme inhibitors.[5] Classical non-steroidal anti-inflammatory drugs (NSAIDs), like aspirin, inhibit both COX-1 and COX-2 isoforms of the enzyme. Interestingly, it is suggested that selective COX-2 inhibitors could provide anti-inflammatory, analgesic, and antipyretic drugs without the unwanted side effects, such as renal failure, typically associated with NSAIDs.[6,7] These selective COX-2 inhibitors might also play a role in preventing or treating some forms of cancer.[8,9] Additionally, these inhibitors may be involved in delaying/slowing the clinical expression of Alzheimer's disease.[10,11]

Indenone compounds have also found use as speroxisome proliferator-activator receptor γ (PPARγ) agonists.[12] The activation of the PPARγ receptor has played an important role in the treatment of type 2 diabetes.[13–15] This type of diabetes, otherwise known as non-insulin-dependent diabetes, accounts for >90% of all cases of this metabolic disorder.[16] In addition to this, indenones have been used as topoisomerase I (Top1) inhibitors.[17] Drugs that have this inhibitory activity have been used for the treatment of cancer.[18–22]

Aside from these significant medicinal applications of indenones, this research is also important because understanding the mechanism behind multicomponent cycloaddition reactions will aid in the development and control of new reactions. Of the various chemistry topics in the literature, cycloaddition chemistry is one that is continually hot due to its wide applicability. This class of reaction is indispensable to the organic chemist in the pursuit of complex natural products or advanced materials for industry.[23] The [5+1+2+1] cycloaddition has not been investigated as much as other cycloaddition reactions (such as the [5+2] cycloaddition between tethered vinylcyclopropanes (VCPs) and alkynes, yielding bicyclo[5.3.0]-fused ring systems) and hence, there is still much to learn about this mechanistically complex reaction.[3]

1.3 In Situ Spectroscopic Studies of Reactions to Observe Intermediates and Elucidate Mechanisms

The use of IR spectroscopy in identifying catalytic intermediates is herein discussed, with particular emphasis on metal-carbonyl catalyzed reactions involving carbonylation and hydroacylation. These reactions are pertinent due to having similar steps

to the cycloaddition presently studied. The intermediates observed in the literature are also often catalyst resting states. However, many important intermediates in catalytic systems are short-lived and cannot be observed using conventional methods. Hence, a discussion is included of how these intermediates can be observed by IR. Finally, although its use was found to be limited in the previous mechanistic study of the [5+1+2+1] cycloaddition reaction, NMR spectroscopy has found great use in the elucidation of intermediates and mechanisms in other metal-carbonyl catalyzed reactions and is also discussed.

1.3.1 In situ Infrared Spectroscopy

The purpose of the in situ infrared (IR) study of this [5+1+2+1] cycloaddition reaction is to observe intermediates along the reaction coordinate that have previously been proposed by DFT calculations.[3] Key steps in the beginning of this reaction are the coordination and insertion of CO and alkyne. Although this particular cycloaddition reaction only requires 1 atm of CO, high pressures of reactant gases are often required for catalytic reactions. Historically, to truly obtain in situ spectra, special high pressure IR (HP-IR) cells had to be developed.[24] One of the first uses of in situ IR spectroscopy to gain mechanistic information was to study the rhodium-complex catalyzed carbonylation of methanol to acetic acid (Scheme 1.2).[25]

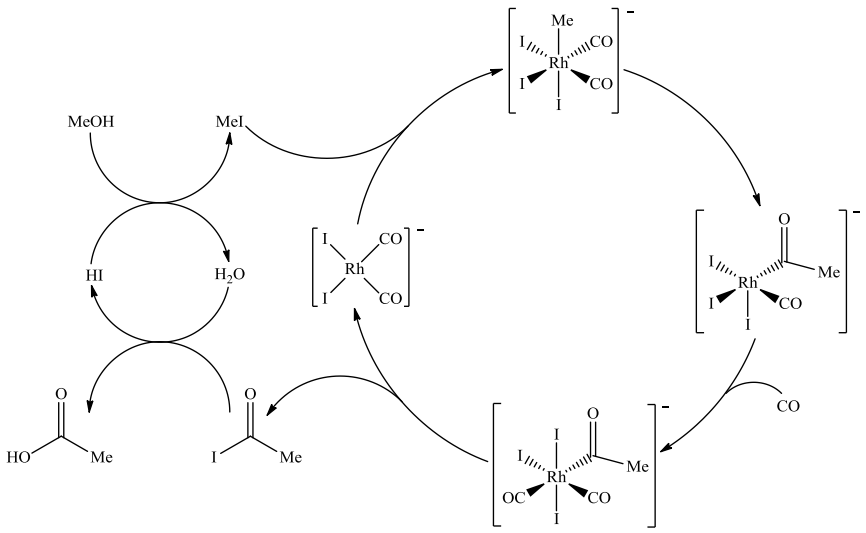

Scheme 1.2: The Rh-catalyzed carbonylation of methanol to acetic acid.[25]

In this study, the reaction of $[Rh(CO)_2I_2]^-$ with methyl iodide was first investigated by IR (not in situ). Peaks for the $[Rh(CO)_2I_2]^-$ ion at 2064 and 1989 cm^{-1}, as well as the CO insertion intermediate (acyl species) at 2062 and 1711 cm^{-1}, were observed. Referencing previous kinetic data,[26] it was strongly suggested that oxidative addition of MeI was rate determining.[25] To have further evidence for the oxidative addition being rate determining, direct spectroscopic observations of the reaction solutions were attempted by using a high pressure, high temperature in situ IR cell. Since only the $[Rh(CO)_2I_2]^-$ ion was observed under these conditions, Forster states that the oxidative addition of MeI is probably the rate determining step of the catalytic cycle (i.e., the reaction is getting bottlenecked at that step, thus that intermediate is observed in situ).[25] This information is pertinent to this thesis, as it suggests that major species observed by in situ IR may be intermediates right before the rate determining step.

Investigation of the synthesis of acetic anhydride from methyl acetate (Scheme 1.3) has shown the presence of this $[Rh(CO)_2I_2]^-$ intermediate as well, with peaks at 2060 and

1990 cm^{-1}.[27] Using in situ conditions at high pressure, this group was also able to observe a peak at 1970 cm^{-1} due to a $Rh(CO)I(PPh_3)_2$ species not present at atmospheric pressure (***Note:*** *this particular species is not observed in Scheme 1.3, as it is part of a second rhodium catalytic cycle not shown for the sake of simplicity*).[27] This study highlights the importance of in situ spectroscopy; although the [5+1+2+1] cycloaddition reaction is performed with only 1 atm of CO, perhaps the species in the catalytic cycle are only observable under high concentrations of CO in solution beneath a CO atmosphere. Taking aliquots of solution to test may result in different species being observed as CO leaves solution.

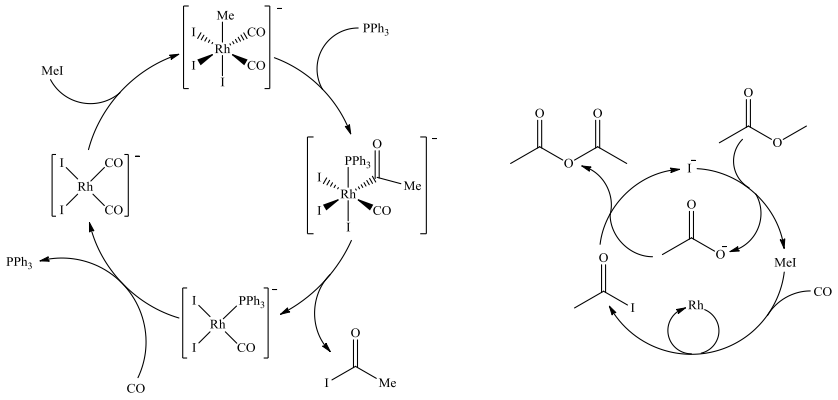

Scheme 1.3: Rhodium and iodide catalytic cycles (left and right, respectively) for the synthesis of acetic anhydride from methyl acetate.[27]

Another group using $[Cp^*Rh(CO)_2]$ as a catalyst for this same methyl acetate reaction (Scheme 1.4) observed the formation of both the expected acyl intermediate (2035, 1690, and 1679 cm^{-1}) and a less active $[Cp^*RhI_2(CO)]$ catalyst (2067 cm^{-1}) by in situ IR.[28] Both species were identified by comparison to literature spectra.[29,30] In another study, the mechanistic aspects of the rhodium/ionic iodide catalysis of two competing reactions (the

reductive carbonylation of methyl formate into acetaldehyde or the homologation of methyl formate into methyl acetate) were studied by in situ IR (Scheme 1.5).[31]

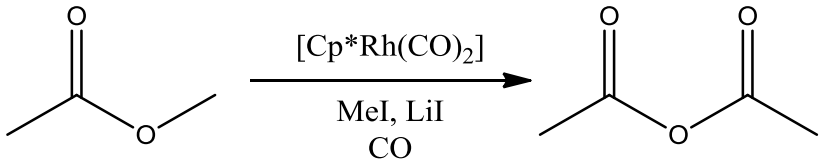

Scheme 1.4: [Cp*Rh(CO)$_2$] catalyzed conversion of methyl acetate to acetic anhydride.[28]

This study was only able to identify the $[Rh(CO)_2I_2]^-$ species by IR, with peaks at 2052 and 1979 cm^{-1}. The group was able to make this identification after comparing with literature data and by preparing an authentic sample. Another peak at 2085 cm^{-1} was unable to be unambiguously identified after several experiments and after searching the literature.[31–35] Collectively, these examples illustrate that the active catalyst can sometimes react to become a less active one, and that definitively assigning a peak to a species can be very difficult.

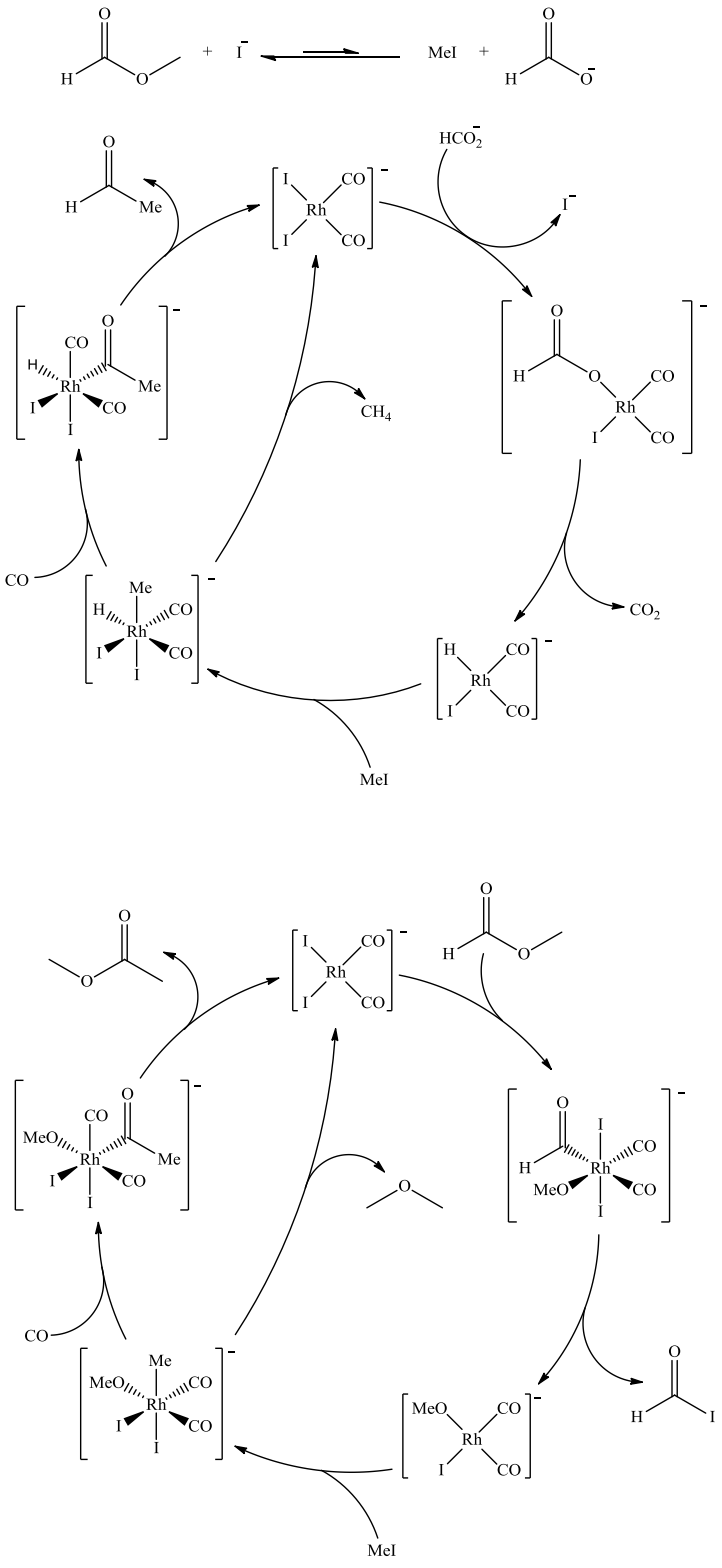

Scheme 1.5: Catalytic cycles for the conversion of methyl formate into acetaldehyde (top) or methyl acetate (bottom).[31]

Finally, another example illustrating the use of HP-IR is the study of the homogeneous rhodium catalyzed hydroformylation of 3,3-dimethylbut-1-ene using $Rh_4(CO)_{12}$, $Rh_6(CO)_{16}$, $Rh_2(CO)_4Cl_2$, $RhCl_3{\cdot}2H_2O$, $CoRh(CO)_7$, and $Co_2Rh_2(CO)_{12}$ clusters as catalyst precursors (Scheme 1.6).[36] It was found that the homometallic rhodium precursors (clusters only containing Rh) all converted into the same catalyst resting state, $[RCORh(CO)_4]$ (R= $-CH_2CH_2C(CH_3)_3$), while the heterometallic precursors (clusters containing both Rh and Co) converted to both $RCORh(CO)_4$ (2111, 2065, 2039, 2020, and 1698 cm^{-1}) and $RCOCo(CO)_4$ (2104, 2044, 2022, and 2003 cm^{-1}) species, suggesting two catalytic cycles (one containing mononuclear rhodium intermediates and the other containing mononuclear cobalt intermediates).[36] The identity of these two catalyst resting states was determined by consulting previous literature.[37–40] Using in situ HP-IR spectroscopy, the concentrations of the one and only observable rhodium intermediate as well as the product, 4,4-dimethylpentanal, were determined, allowing for kinetic information to be obtained.[36] Kinetic results showed negligible contribution from the Co intermediate to the overall rate. A one-to-one relationship between the concentration of the Rh intermediate and the rate of product formation was found for all reactions (regardless of whether a homometallic or heterometallic catalyst precursor was used). These mixed-metal (Co-Rh) catalysts also showed higher activity. This activity was ascribed to the facile fragmentation of these complexes to generate reactive fragments that give rise to catalytic cycles involving only one metal (as opposed to cluster catalysis or a binuclear elimination mechanism).[36]

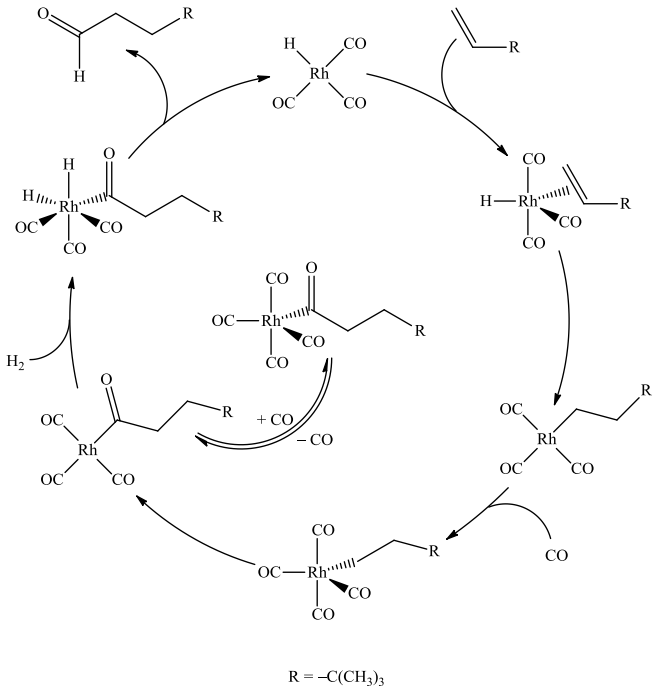

Scheme 1.6: The catalytic cycle for the hydroformylation of 3,3-dimethylbut-1-ene to 4,4-dimethylpentanal.[36,41]

Not only does this study illustrate the use of in situ IR to identify a Rh carbonyl catalyst resting state, but it also demonstrates the use of IR to obtain kinetic information. The study of the [5+1+2+1] cycloaddition will not use in situ IR for kinetic purposes due to unstable peak intensity of the IR probe used; nonetheless, it is worth mentioning this important application of IR.

1.3.2 Using In Situ Infrared Spectroscopy to Observe Short-Lived Intermediates

These previous examples largely exemplify the use of in situ IR to observe catalyst resting states. However, how would one observe reactive, short-lived intermediates? A paper published by Simpson et al.[42] demonstrates the use of UV photolysis in conjunction with low temperature, liquefied noble gases (Xe or Kr doped with 5% Xe) to give the first spectroscopic evidence of $[Cr(CO)_5Xe]$ in solution (Scheme 1.7).

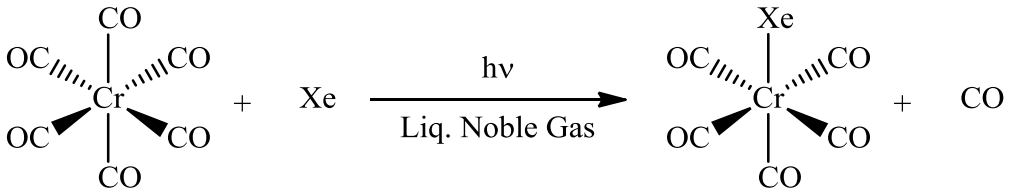

Scheme 1.7: Formation of the $Cr(CO)_6Xe$ species by UV photolysis in low temperature, liquefied noble gas.[42]

It is worth noting that Xe has a stronger interaction than Kr and therefore $[Cr(CO)_5Xe]$ is formed for much longer than $[Cr(CO)_5Kr]$. Coordinatively unsaturated metal carbonyl species are known to be very reactive, but under the experimental conditions of this paper (−98 ºC) this species is stabilized by noble gas solvation. The species was then able to be detected by conventional in situ IR and was found to have a half-life of ca. 2 s. Without this stabilizing solvation, much faster scanning techniques would have to be used (on the order of microseconds) as opposed to the 17 s scans used in this paper.[42] Referencing previous literature[43–45], it was shown that the observed frequency bands closely match those of the matrix-isolated $[Cr(CO)_5Xe]$ and are significantly different than those of impurities. Other studies have been performed along these lines.[46,47]

Another way to observe reactive intermediates is to use IR with very short scanning intervals. A review has been published covering the use of a combination of flash photolysis and time resolved infrared (TRIR) spectroscopy to characterize structures and reactivities of short lived and elusive intermediates along the reaction pathway of thermal CO migratory insertion.[41] In this type of insertion, the transient species under catalytic conditions are elusive due to low steady-state concentrations. Laser flash photolysis is used to produce non-steady-state concentrations of these intermediates, starting with the acyl compound (CO already inserted) and working backward along the reaction coordinate.

This photolysis technique (used on a Mn model system) ejects a CO ligand, allowing reverse alkyl migration (Scheme 1.8).[41]

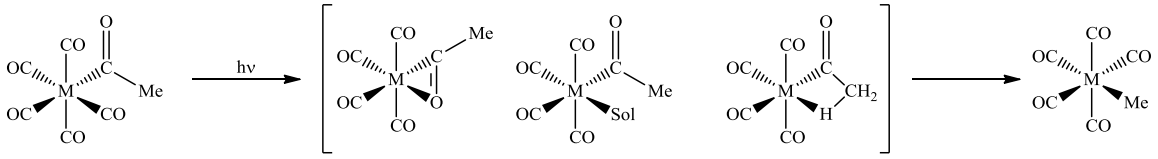

Scheme 1.8: Reverse alkyl migration induced by flash photolysis of an acyl metal-carbonyl species, where Sol = Solvent.[41]

TRIR was used to investigate the nature of the formed intermediate, with peaks forming and disappearing on the microsecond scale. Kinetic data of this photolytically formed species was then compared to that of the thermally formed intermediate to determine whether this technique provides a reasonable model of thermal CO insertion. Studies on cobalt carbonyl catalysts were also performed.[41] Overall, these studies concluded that the intermediate formed from the photodissociation of the acyl compound was an equilibrium ensemble of several species (one containing coordinated solvent). Using the Mn model system, the kinetic data supported the assertion that the photochemically generated intermediates are likely the same as those formed thermally (at least when performed in THF). Furthermore, spectral and kinetic data showed that the behaviour of the Co intermediates largely paralleled that of the Mn intermediates.[41] Several other studies have been performed using TRIR spectroscopy to observe these elusive intermediates of carbonylation.[48–50]

This thesis will not use liquid noble gases or TRIR spectroscopy to observe highly reactive and short-lived metal carbonyl species, as these conditions and equipment are outside the means of our research lab. However, these previously highlighted studies give

a good overview of what can be done to observe such species spectroscopically. This thesis will only be able to observe catalyst resting states, considering that in situ conditions are at elevated temperatures for the [5+1+2+1] cycloaddition reaction and the IR probe being used has a minimum scanning interval of 15 seconds (far from the microsecond intervals used in TRIR).

1.3.3 In Situ NMR Spectroscopy

NMR is one of the most powerful tools available to the organic chemist for determination of compound structure and reaction rates. As mentioned before, high pressures of reactant gases are often required for catalytic reactions. Like IR, to truly obtain in situ spectra, high pressure (HP) NMR had to be developed.[24] For example, special probes (e.g. modified hydrostatic probes) and tubes (e.g. sapphire tubes) must be used for NMR when involved in a high pressure environment. HP-NMR has found use in the mechanistic elucidation and confirmation of transition-metal catalyzed activation of molecular hydrogen, ethylene polymerization, hydroacylation of ethylene, thermal degradation of PVC, and coal liquefaction.[51] Additionally, HP-NMR was successfully used to investigate exchange of hydrogen, carbon monoxide, carbon dioxide, and coordinated cyclopentadienyl ligands in equilibrium systems.[51] In studying the catalytic synthesis of ethylene glycol from syngas (mixture of CO and H_2), the reaction of $[Rh_{12}(CO)_{30}]^{2-}$ with CO at high pressure and in the presence of hydrogen (in situ conditions) was monitored by ^{13}C HP-NMR.[52] Both this species and $[Rh_5(CO)_{15}]^-$ were known to be present in the catalytic mixture, but it was unknown at the time whether these clusters were themselves the catalyst or if they were in equilibrium with catalytically active species.[53] The group was trying to determine if $[Rh_{12}(CO)_{30}]^{2-}$, when placed under in situ conditions, would form

any new, previously unidentified species. A clean conversion of $[Rh_{12}(CO)_{30}]^{2-}$ to $[Rh_5(CO)_{15}]^-$ was observed by NMR, with the $[Rh_5(CO)_{15}]^-$ species being identified through comparison to the literature.[54] This study presents one of the first examples of using in situ HP-NMR to identify possible metal carbonyl compounds present in a catalytic solution.[52] Around a decade later, another group made use of a bulky trialkylphosphine for this reaction. This addition of the trialkylphosphine was found to enhance both the activity and stability of the Rh carbonyl catalyst (Scheme 1.9).[55]

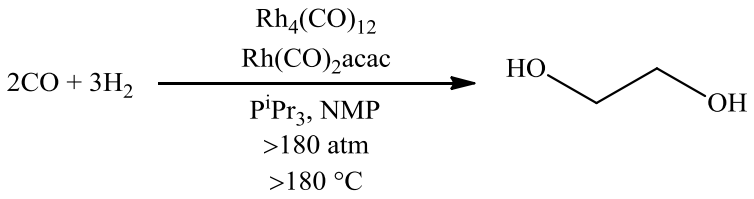

Scheme 1.9: Direct route from syngas to ethylene glycol using a bulky triisopropylphosphine catalyst.[55]

Reactive and elusive species have also been identified at cold temperature by HP-NMR. A direct intermediate for CO insertion (a square-planar palladium diphosphine complex with methyl and carbonyl groups in a *cis* configuration, Compound **3**) was identified at 183 K using the chemical shift values and coupling constants of ^{31}P and ^{13}C HP-NMR (Scheme 1.10).[56]

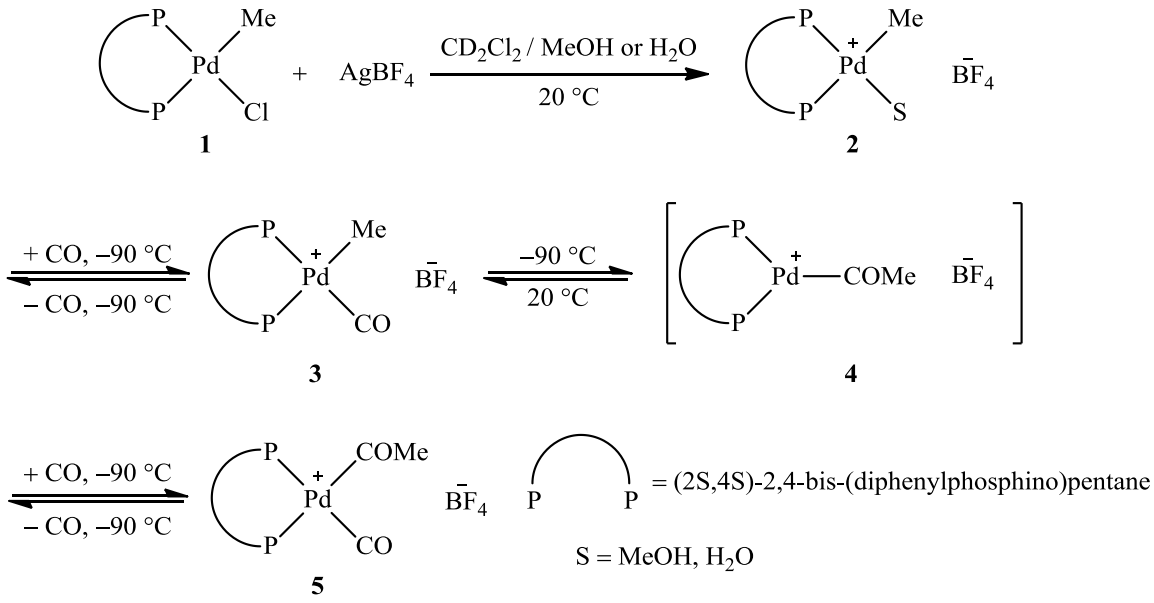

Scheme 1.10: Reaction sequence for the CO insertion of the palladium diphosphine complex.[56]

Such compounds have previously been elusive due to the fast migratory insertion of CO to give the acyl species; the lifetime of this species was found to be ca. 8 h at 183 K. The acetyl carbonyl complex **5** (formed from CO insertion followed by another CO coordination) was also identified by chemical shift values and coupling constants as well as IR.[56] HP-NMR kinetic studies performed using increased CO pressure found that formation of the *cis* methyl carbonyl complex **3** is accelerated while the rate of formation of the acetyl carbonyl complex **5** did not change. This observation is consistent with the proposed mechanism.[56] Isotopic labelling is another particularly useful avenue when investigating mechanisms. For example, ^{13}C and ^{2}H labelling has been used to elucidate the mechanism of the reaction between benzaldehyde and ethene using an indenyl Rh catalyst (Scheme 1.11).[57]

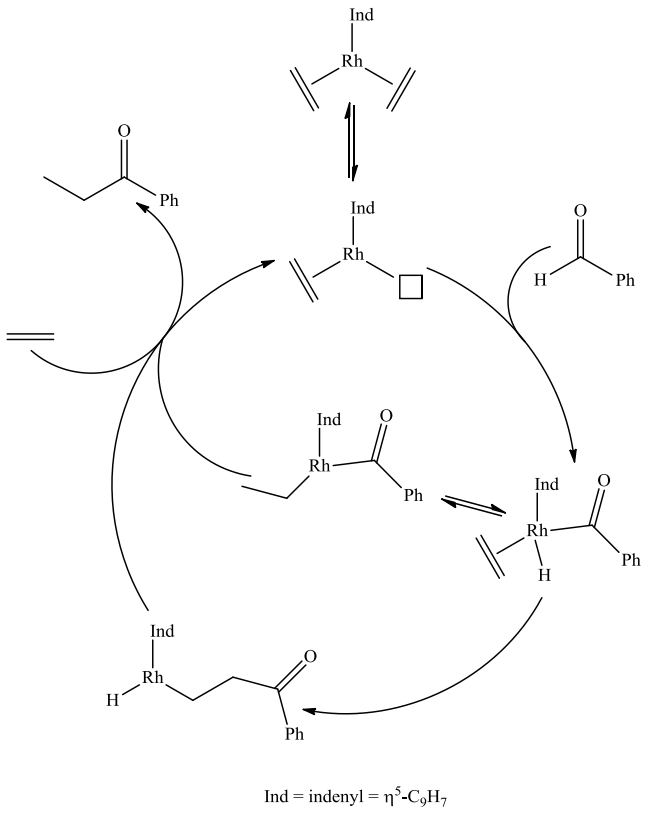

Scheme 1.11: Proposed catalytic cycle for the Rh-catalyzed hydroacylation of benzaldehyde and ethene to propiophenone.[57]

This thesis will not make use of NMR and isotopic labelling for structural determination of intermediates. Nevertheless, it is worth mentioning that NMR is a powerful spectroscopic technique that has contributed to a wealth of knowledge regarding reaction intermediates and mechanisms.

An inherent problem with NMR spectroscopy is that it is a relatively insensitive technique. Importantly, species that are present in the catalytic solution are sometimes different when higher concentrations are used for NMR measurements.[24] As previously mentioned, this problem of NMR insensitivity became apparent when studying the [5+1+2+1] cycloaddition reaction by NMR: higher concentrations were needed to observe the Rh catalyst intermediates, but higher concentrations also led to the formation of an

inactive, bimetallic Rh species that did not allow the reaction to proceed.[4] IR spectroscopy has much greater sensitivity than NMR, giving it suitability for the study of catalytic solutions.

1.4 Processing and Computational Methods to Aid in Peak Assignment

Making peak assignments to reaction intermediates when investigating multi-component mixtures by in situ IR spectroscopy can be very difficult. Firstly, multi-component mixtures can often have overlapping peaks in their IR spectra. Before any peak assignment can be made, these peaks need to be separated. A processing method of second derivative analysis is herein mentioned to meet this challenge. Additionally, once the peaks have been properly separated, it is challenging to make assignments to particular species without the appropriate reference spectra. Two computational methods to address this issue of peak assignment, Band-Target Entropy Minimization (BTEM) and vibrational scaling factors, are discussed.

1.4.1 Second Derivative Data Processing

A frequently encountered difficulty when using in situ IR spectroscopy is to observe low intensity peaks in the spectra and to separate overlapping peaks so that they can be properly identified. A paper published by Whitbeck in 1981 describes the use of second derivative analysis of IR spectroscopy to analyze trace absorbers in a spectrum.[58] Using this type of data treatment, sharp spectral features are enhanced while broad features (like a gradually curving background) are lessened. A complicated mathematical process (cubic spline interpolation) was used to calculate the first and second derivatives. To illustrate the usefulness of this technique, second derivative data treatment was performed

on a high resolution (0.25 cm^{-1}) spectrum of gaseous CO.[58] This resulted in great enhancement of the CO peaks and of the finer features of the spectrum. However, these features were enhanced along with noise. Since air was not purged from the spectrometer before addition of CO, trace absorbers from the air were also enhanced.[58] To demonstrate the sensitivity of second derivative analysis toward trace gases, the CO was purged from the instrument with N_2 and a spectrum was obtained. Expanding the scale 40 times showed virtually no CO peaks, but a second derivative analysis clearly showed the presence of the trace gas without scaling. This study clearly illustrates that second derivative analysis is a good method to enhance finer features of a spectrum as well as trace components. However, the enhancement of noise in the spectra could be problematic for identifying peaks.[58]

Further information about second derivative spectroscopy was found in a technical bulletin published by Owen in 1995 for Agilent Technologies.[59] This bulletin outlines the uses of derivative spectroscopy for UV-Vis, although the information mentioned is equally applicable to IR. The appearance of derivatized functions is first described for both odd-order and even-order derivatives. The derivative order plus one is equal to the number of observed bands.[59] Simple linear interpolation between adjacent wavelengths and polynomial fitting to a window of data points are two mathematical methods discussed to obtain such derivatives. An important application is the enhanced resolution of peaks with very similar λ_{max} values, since the centroid bandwidth decreases (i.e., the bands become more narrow) with increasing derivative order. This bandwidth narrowing facilitates multi-component analysis by separating overlapping peaks.[59] Additionally, broad bands are suppressed relative to sharp bands, with increasing derivative order leading to increased suppression. This bulletin states that a downside to derivative data treatment is the

decreasing signal-to-noise ratio as the derivative order increases. This negative consequence arises from the fact that the sharpest features in the spectrum are always contained in the noise (and are therefore enhanced relative to broader features).[59]

This information on second derivative treatment of data is quite pertinent to this thesis because it provides a way to observe the presence of minor species in the catalytic solution. Additionally, any regions of the IR spectrum that have overlapping peaks may be better resolved using this technique. Better resolution and separation of peaks is absolutely necessary for unambiguous assignment, which is one of the main focuses of this thesis. This information is of additional importance because it is vital to know how the data treatment will affect the appearance of the spectrum. For instance, are new peaks appearing due to better resolution and separation, or are they appearing because they are satellite bands resulting from the second derivative process? Furthermore, these publications warn of decreased signal-to-noise ratios from this data treatment. Therefore, gains made in separating overlapping peaks may be lost when trying to differentiate low intensity peaks from the baseline noise. Of the various methods to calculate the first and second derivatives, linear interpolation between adjacent wavelengths appears to be most appropriate for this thesis due to its simplicity and ease of use.

1.4.2 Band-Target Entropy Minimization Computations

As shown by the above examples, more often than not the peaks are identified through comparison to literature spectra. However, how would one unambiguously assign peaks when reference spectra are not available? A paper published by Chew et al. describes the development and use of a band-target entropy minimization (BTEM) algorithm to

recover unknown pure component spectra of the constituent compounds of mixtures.[60] To illustrate the usefulness of this technique, the FTIR data of a mixture of $Rh_4(CO)_{12}$ and $Rh_6(CO)_{16}$ was processed using the BTEM algorithm. The use of this algorithm resulted in remarkably accurate reconstructions of pure $Rh_4(CO)_{12}$ and $Rh_6(CO)_{16}$ spectra. Notably, this method was able to recover these pure component spectra despite the presence of highly overlapping bands.[60] Even the spectrum of $Rh_6(CO)_{16}$ solid (present in very small amounts in the form of insoluble suspended particles) was able to be reconstructed. The BTEM algorithm was found to outperform other spectral reconstruction methods such as SIMPLISMA, IPCA, and OPA-ALS. Reconstructions using these other methods either failed outright or did not produce spectra of similar quality to BTEM. Overall, this method is very advanced but has great potential for use in the field of in situ IR spectroscopy where absolutely no a priori information is available with regard to the intermediates/constituents of the reaction solution.[60] The BTEM separation of Rh carbonyl species to give the respective pure component spectra is relevant to this thesis, as using this technique may enable the identification of similar Rh carbonyl species in the catalytic solution. However, the advanced mathematics needed to use this technique is beyond the scope of this thesis. Additionally, from the previous DFT study of the [5+1+2+1] cycloaddition reaction, a priori information about possible species along the reaction coordinate is available.

1.4.3 Vibrational Scaling Factor Computations

Noting that structural assignment of intermediates along a reaction coordinate can be difficult due to lack of reference spectra, it has been recognized that calculation of vibrational frequencies is a very useful tool for peak assignment. There are systematic differences between the computed and experimental vibrational frequencies, and scaling

factors to correct for approximations inherent in calculations has been extensively studied.[61–65] A study by Kohls and Stein in 2017 set out to determine vibrational scaling factors for Rh(I) carbonyl compounds.[66] A set of 45 carbonyl containing Rh(I) complexes (with available IR data) was selected from the literature as the experimental set. Models of these complexes were created at the DFT level using BP86 and B3LYP functionals, with the def2-TZVP basis set being used for both.[66] Importantly, it has been shown that the accuracy of calculated frequencies is not necessarily improved by using larger basis sets.[63] The average absolute error for the unscaled BP86 and B3LYP calculated frequencies was found to be 1% and 3.5%, respectively.[66] BP86 frequencies could be used without scaling (slight errors were present), but more than one third of the B3LYP errors were greater than 70 cm^{-1}. Vibrational scaling factors for BP86/def2-TZVP and B3LYP/def2-TZVP were calculated to be 1.0074 and 0.9662, respectively. After scaling, both methods could properly reproduce the experimental CO frequencies.[66] To illustrate the usefulness of this technique, the group compared calculated spectra of two different stereoisomers of a pre-catalyst used in the Rh-catalyzed hydroformylation reaction to an experimental spectrum of the (e,e) stereoisomer (Figure 1.1).

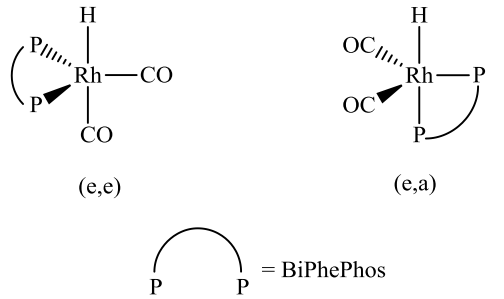

Figure 1.1: The (e,e) and (e,a) stereoisomers of a pre-catalyst used in hydroformylation of long chain olefins. The bidentate phosphite ligand can coordinate in two different ways, thus resulting in the two different stereoisomers. The dissociation of a CO ligand activates this catalyst.[66]

This comparison resulted in the successful assignment of the structure. Finally, this paper notes that global scaling factors (applicable to the entire IR range) found in the literature are not recommended for CO stretches of transition metal carbonyl complexes because these can lead to even larger deviations from experimental frequencies (instead of correcting them).[66] In comparison to BTEM, this method appears to be the more accessible for unambiguous peak assignment.

1.5 Aim of this Thesis

The overall goal of this work is to determine if the previously calculated intermediates along the cycloaddition reaction pathway can be observed by in situ infrared spectroscopy. Peak assignments of the intermediates will be aided by second derivative data analysis as well as scaling factors applied to computationally derived IR spectra. Further computational work will be performed to determine if the cycloaddition reaction can proceed as a bimetallic rhodium species to some extent. Additionally, the energetics of why the reaction does not proceed after forming the bimetallic species will be explored computationally.

Chapter 2 – Results & Discussion

2.1 Synthesis of VCP and Modifications to Previous Procedure

To begin the investigation of the [5+1+2+1] cycloaddition reaction, the VCP starting material first had to be synthesized (see Scheme 2.1).

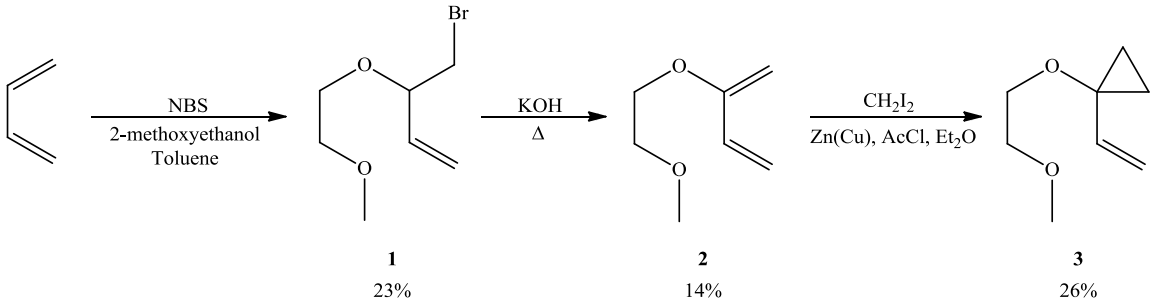

Scheme 2.1: Multistep sequence for the synthesis of VCP, including isolated yields.

In order to form the halo-alkoxide **1**, 1,3-butadiene was reacted with NBS and 2-methoxyethanol in toluene. The subsequent elimination using KOH gave diene **2**. This elimination was modified so that the addition of base was performed with the round-bottom flask fully submerged in ice. Previous trials of this reaction resulted in the reaction flask becoming extremely hot, so this modification was made to the procedure out of safety concerns. Finally, a Simmons-Smith cyclopropanation was performed to give the final vinylcyclopropane **3**. It is worth mentioning that the cyclopropanation reaction time of 7 hours reported herein is drastically different from the 30 minutes reported by Mbaezue.[4] Thus, monitoring of the reaction by TLC was found to be critically important to determine reaction completion. This difference in reaction kinetics is surmised to be partly due to a change in reactant concentration, as the reagent amounts reported in Chapter 5 have been scaled down by a factor of 0.8 relative to the amounts reported by Mbaezue, while the

volume of solvent used in both preparations remained the same. Another factor affecting the reaction kinetics might be the quality of the reagents. Since the Mbaezue procedure was performed in the same laboratory as this thesis and used the same chemicals, it is possible that perhaps some of the materials used for this reaction had degraded over time. The acetyl chloride and diiodomethane were both tested by ^{1}H NMR and showed no sign of decomposition. Additionally, the copper (I) chloride that was presently used had been stored under the inert atmosphere of a glovebox. This compound qualitatively showed no signs of oxidation to copper (II) chloride, as an impure sample of copper (I) chloride will appear green due to the present of copper (II) chloride dihydrate. The zinc metal that was used had simply been stored open to the atmosphere, and perhaps a zinc oxide coating had developed over time and had not been sufficiently removed after the purification procedure reported by Simmons and Smith.[67]

Due to the relatively low yield of this cyclopropanation reaction (26%) and the small amount of VCP that was isolated (198.3 mg), a modification was made to the Mbaezue procedure to eliminate the vacuum distillation of VCP. ^{1}H NMR showed that the product was sufficiently clean, and there was concern that a significant amount of product would be lost in the vacuum distillation.

The methods reported herein (and further described in Chapter 5) were modified from a procedure reported by Mbaezue in 2017.[4] The procedure reported by Mbaezue was itself an optimization of a procedure reported by Wender et al. in 2000.[68]

2.2 Crystallization of a Bimetallic Rhodium Intermediate

During the spectroscopic investigation of the [5+1+2+1] cycloaddition reaction mechanism, Mbaezue found by ^{1}H NMR that when 1 equiv. of VCP was reacted with 1 equiv. of $[Rh(CO)_2Cl]_2$ under N_2, two species were present. The existence of these species was suggested by two methoxy peaks at 3.13 and 3.15 ppm, as shown in Figure 2.1. This mixture of two species subsequently converged to only one species upon the addition of CO to solution, as suggested by the single methoxy peak at 3.15 ppm (see Figure 2.2). This single species was crystallized and found to be a bimetallic rhodium intermediate (see Figure 2.3).

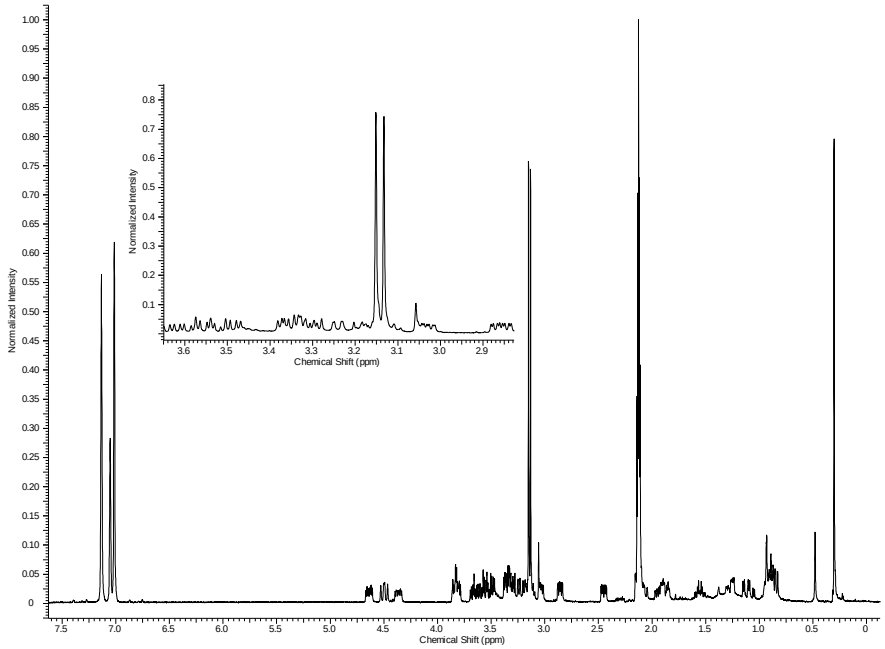

Figure 2.1: ^{1}H NMR (300 MHz, toluene-d_8) spectrum of the mixture of rhodium intermediates from the reaction of VCP with 1 equiv. of $[Rh(CO)_2Cl]_2$.

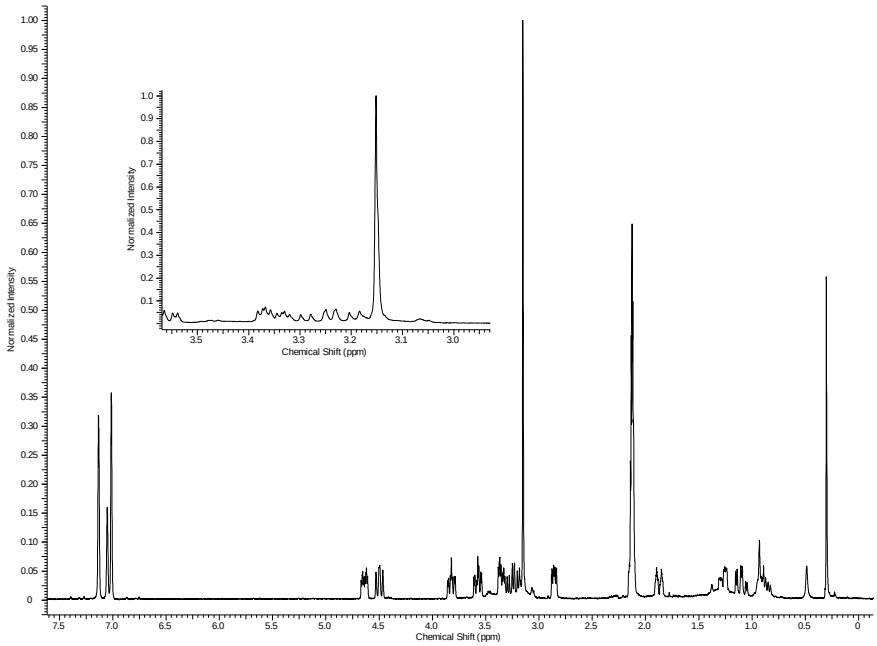

Figure 2.2: ^{1}H NMR (300 MHz, toluene-d_8) spectrum of a single rhodium intermediate from the reaction of VCP with 1 equiv. of $[Rh(CO)_2Cl]_2$ and excess CO.

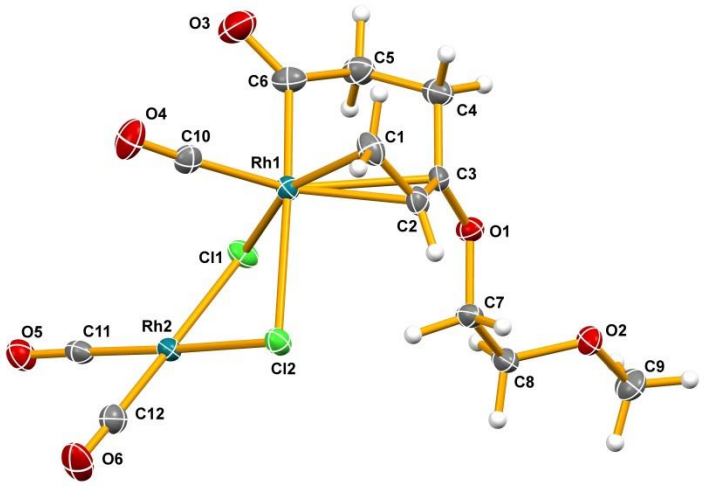

Figure 2.3: Solid state structure of the bimetallic rhodium intermediate **BM1**. Thermal ellipsoids are drawn at the 50% probability level.

Later ^{1}H NMR experiments by Mbaezue suggested that **BM1** is an off-cycle intermediate. For instance, ^{1}H NMR showed that when **BM1** was heated for 44 hours, from 60°C-85°C, no change had occurred in the spectrum. From this, it was concluded that CO insertion in the absence of alkyne did not occur, even at elevated temperatures. In other words, a second carbonyl ligand would not insert to allow for the [5+1+1+2] reaction pathway. Referring to Figure 2.3, it can be seen that C10 of the carbonyl ligand is in a cis configuration to C1. Therefore, although CO insertion is not observed, the CO ligand appears to be in the correct geometry for insertion. Additionally, it was shown by Mbaezue that the reaction of **BM1** with various alkynes would not proceed, therefore suggesting that the reaction through the [5+1+2+1] pathway was not possible either from this species. It is important to note that the reaction successfully proceeded when **BM1** was diluted with more solvent in the presence of CO and alkyne. This observation suggests that the formation of the bimetallic species is reversible, and it also suggests that the cycloaddition can only fully proceed via a monometallic reaction mechanism.

Having identified one of the rhodium species in this mixture, it was thought that crystallizing the mixture of the two species might allow the other unknown compound to crystallize. After months of slow evaporation, thin, bright red, needle-like crystals were obtained from dark brown oil. However, these crystals were found to be the starting rhodium dimer catalyst, $[Rh(CO)_2Cl]_2$. ^{1}H NMR was used to determine that the mixture of the two rhodium intermediates had oiled out. In other words, the ^{1}H NMR spectrum of the oil matched that of Figure 2.1.

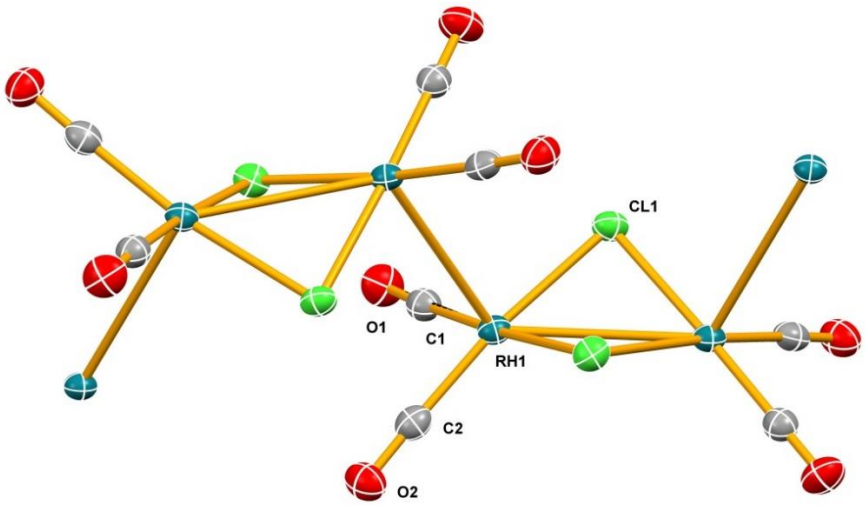

Figure 2.4: Solid state structure of the rhodium dimer catalyst. Only the atoms that are crystallographically unique have been labelled. Thermal ellipsoids are drawn at the 50% probability level.

2.3 Test of the Cycloaddition Reaction

After synthesizing VCP, it was important to test if the [5+1+2+1] cycloaddition reaction would be reproducible in our laboratory. By following the Wender procedure[2] for the cycloaddition reaction, clear, pale yellow/brown, rod-like crystals were obtained from solution after ca. 40 hours of reaction time. These crystals were identified as the desired hydroxydihydroindanone cycloaddition product, as shown in Figures 2.5 and 2.6.

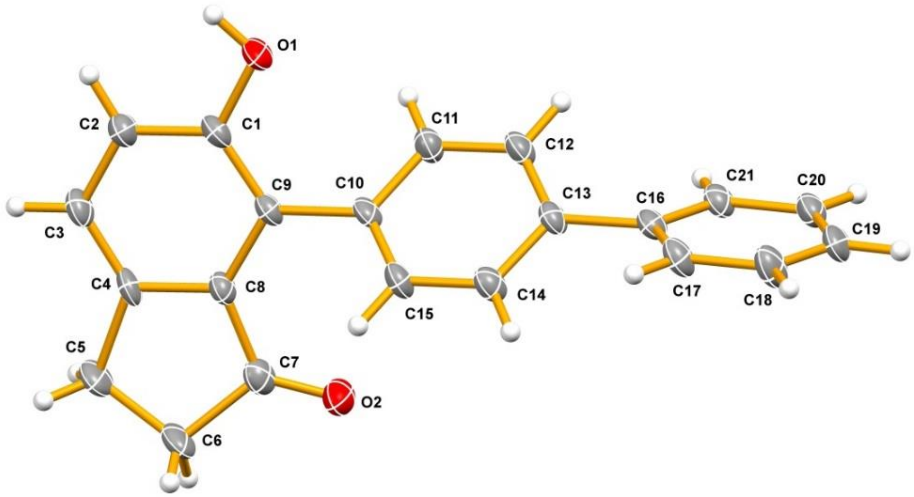

Figure 2.5: Solid state structure of the hydroxydihydroindanone cycloaddition product. Thermal ellipsoids are drawn at the 50% probability level.

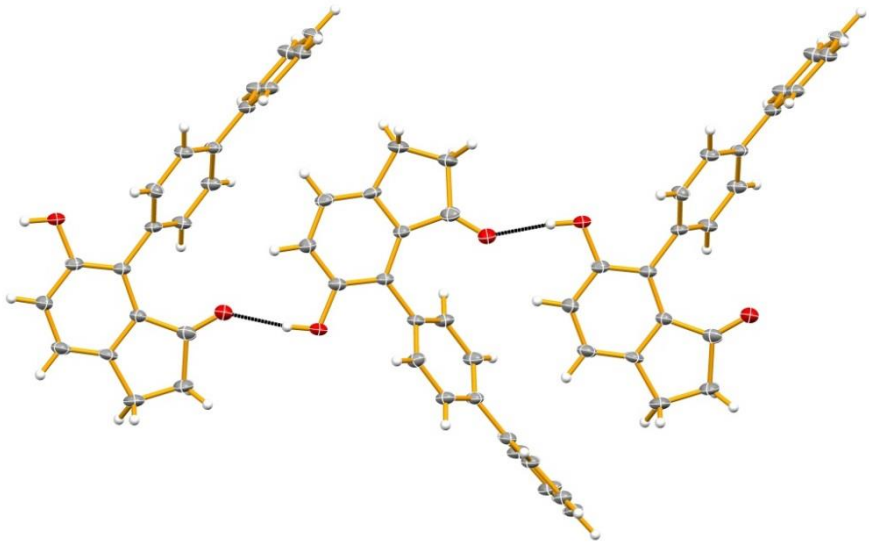

Figure 2.6: Solid state structure of the hydroxydihydroindanone cycloaddition product illustrating the OHO hydrogen bonding network. Thermal ellipsoids are drawn at the 50% probability level.

Having this structure was vitally important, as it gave unambiguous evidence that the reaction was reproducible before further studies were carried forward. Additionally, it was important to have a pure spectrum of the cycloaddition product before beginning the in situ IR studies so that the carbonyl peak of the product, which was expected to grow into the in situ spectra as the reaction progressed, could be unambiguously assigned.

2.4 In Situ Spectroscopic Studies

As previously stated, NMR studies of the [5+1+2+1] cycloaddition reaction that were performed by Mbaezue used higher catalyst loadings in an attempt to observe reaction intermediates without the presence of VCP (noting that any excess Rh dimer catalyst would not appear in a ^{1}H NMR spectrum). However, these higher loadings resulted in the formation of the unreactive bimetallic species **BM1**, as seen in Figure 2.3. As mentioned in the introduction, infrared spectroscopy was thought to be a promising avenue of investigation for this reaction, as it is more sensitive than NMR and thus, intermediates might still be observed with the use of lower catalyst loadings.

Furthermore, this reaction also lent itself well to IR spectroscopy due to the nature of the intermediates. Firstly, carbonyl ligands result in intense IR peaks due to a large change in dipole moment when the C-O bond stretches. Secondly, CO peaks on a metal center are very sensitive to their chemical environment. This sensitivity is due to a concept known as π-backbonding, wherein the filled *d*-orbitals of the metal center (in this case, rhodium) donate electron density into the empty π*-orbital of the carbonyl ligand (see Figure 2.7). Metal centers with more electron density participate more in *d*-π* backbonding. This phenomenon results in a stronger M-C bond, but the C-O bond order is

reduced due to electron density being donated into its antibonding orbital. This lower C-O bond order can then be spectroscopically observed by IR since the wavenumber of the stretch is subsequently reduced.

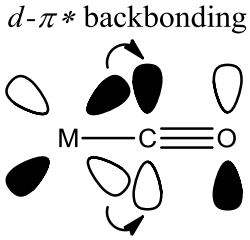

Figure 2.7: *d-π** backbonding in a metal carbonyl compound (M = metal center).

Conversely, a less electron rich metal center participates in less *d-π** backbonding, thus resulting in relatively weaker M-C bonds and relatively stronger C-O bonds in comparison to a compound with strong *d-π** backbonding. It was hypothesized that since the intermediates along the reaction coordinate of the [5+1+2+1] cycloaddition reaction should have varying electron densities at the rhodium center, it should be possible to monitor the progress of the reaction through observation of the carbonyl region in IR.

2.4.1 Study of the [5+1+2+1] Cycloaddition Reaction

To study the cycloaddition reaction by in situ IR, low catalyst loadings (2.7 mol % relative to alkyne) were used to ensure the reaction proceeded. To see the peaks with respect to sequential reagent addition and time, see Table 2.1. The addition of rhodium dimer catalyst resulted in the appearance of two peaks at 2081 and 2003 cm^{-1}. Subsequently, the addition of VCP to this solution resulted in a shift of these peaks to 2077 and 1999 cm^{-1}. After this, 4-ethynylbiphenyl was added to solution, resulting in no change of the spectrum (noting that the change of wavenumber from 2077 to 2073 cm^{-1} is not

deemed significant, as the resolution of the spectrometer is only 4 cm^{-1}). Finally, CO was bubbled into solution, resulting in a spectrum with peaks at 1999, 2021, and 2073 cm^{-1} in the carbonyl region.

Table 2.1: In situ IR trial of the cycloaddition reaction in toluene using 2.7 mol % of Rh dimer catalyst relative to alkyne to ensure the reaction proceeded.

Note	**Wavenumber (cm^{-1})**				
Rh cat Addition		2003		2081	
VCP Addition		1999		2077	
4-ebp Addition		1999		2073	
CO Addition		1999	2021	2073	
Heating 5 h		1999	2021	2073	
Heating 10 h		1999	2021	2077	
Heating 15 h		1999	2021	2073	shoulder
Heating 20 h		1999	2021	2077	shoulder
Heating 25 h		1999	2021	2077	shoulder
Heating 30 h	1715	1999	2021	2077	2088
Heating 33 h	1715	1999	2021	2073	2088
Heating 35 h	1715	1999	2021	2073	2088

Heating this solution for 32 hours at 60 ºC resulted in no change to these peaks. However, second derivative analysis revealed the emergence of a shoulder peak after ca. 15 hours of heating. This shoulder was eventually resolved to 2088 cm^{-1}. It is worth noting that this peak may just be background noise, as the signal-to-noise ratio after second derivative analysis is very low. Additionally, after ca. 30 hours of heating, a peak at 1715 cm^{-1} began to grow into the spectrum. This peak was assigned to the carbonyl stretch of the

hydroxydihydroindanone cycloaddition product through comparison to a pure IR spectrum of the product previously obtained. A pure spectrum of CO in toluene was also obtained, which had two peaks at 1999 and 2021 cm^{-1}. The cycloaddition reaction was set to run overnight but went dry early the next morning, despite sealing the three-neck round bottom with septa and parafilm. According to Wender, the cycloaddition reaction is complete after 30 hours. Thus, this reaction most likely completed before the solvent evaporated.

Having the reaction go dry was unintendedly beneficial from a spectroscopic standpoint, as it concentrated the solution and allowed the observation of the carbonyl peak corresponding to the product (and thereby illustrating that the reaction was in fact working). The cycloaddition product is sparingly soluble in toluene, and thus it is expected that it would only begin to appear once the solution had been concentrated. Since the carbonyl stretching frequency of the hydroxydihydroindanone cycloaddition product is an important spectroscopic handle, at first it may seem unintuitive to use a solvent that the product is insoluble in. However, studies performed by Wender et al. in 2005 discovered that there is a beneficial effect to using solvent systems that result in the precipitation of the product.[2] Control experiments illustrated that the product interferes with the efficiency of the four component process. Additional controls indicated that the VCP was unstable in the reaction conditions while in the presence of the cycloaddition product.[2]

The change in peak wavenumbers with the addition of the VCP to the rhodium catalyst solution (see Table 2.1) was found to be insignificant, as the resolution of the instrument is 4 cm^{-1} and the wavenumbers change by 4 cm^{-1}. In other words, it cannot be stated with confidence that the wavenumber has changed. It has previously been demonstrated by Mbaezue that VCP reacts with rhodium dimer catalyst almost

immediately. Thus, this result suggests that IR spectrometers in general do not have the resolution needed to differentiate the CO peak positions of this reaction. (i.e., the reaction is proceeding but the instrument cannot resolve the small wavelength changes of the peaks). This result may also indicate that the reaction is being bottlenecked at a rate determining step, or RDS, and therefore, the only species observed is the one right before the RDS (i.e., the concentration of the species right before the RDS is increased due to the reaction being bottlenecked at that step). This explanation invoking the RDS would agree with similar observations made by Forster when studying the rhodium-complex catalyzed carbonylation of methanol to acetic acid (as discussed in the introduction).[25]

2.4.2 Study of the [5+1+2+1] Cycloaddition Reaction with N_2 Sparging

It was hypothesized that if nitrogen gas was periodically sparged into the reaction solution, perhaps the peaks due to free CO could be removed from the spectrum, thus facilitating the observation of peaks due to reaction intermediates. However, when this sparging technique was applied while obtaining in situ spectra, not only was it unsuccessful in removing the free CO peaks, but the overall signal-to-noise ratio of the spectra was reduced (before second derivative analysis). It is unknown why sparging an inert gas through solution would affect the noise of the IR spectrum. However, why this sparging did not remove the free CO peaks was further investigated.

2.4.3 Study of the Solubility of CO in Toluene

To test the difficulty of removing CO peaks from an IR spectrum, an in situ IR trial was performed wherein CO was bubbled into solution for ca. 5 minutes, followed by nitrogen being sparged through solution to remove the dissolved CO. It took ca. 5 hours of

nitrogen sparging to remove the CO peaks, with the intensity of these peaks decreasing asymptotically (see Figure 2.8). This test illustrated the high solubility of CO in toluene, and further illustrated that removing the CO peaks from the in situ IR spectra would not be possible for this study.

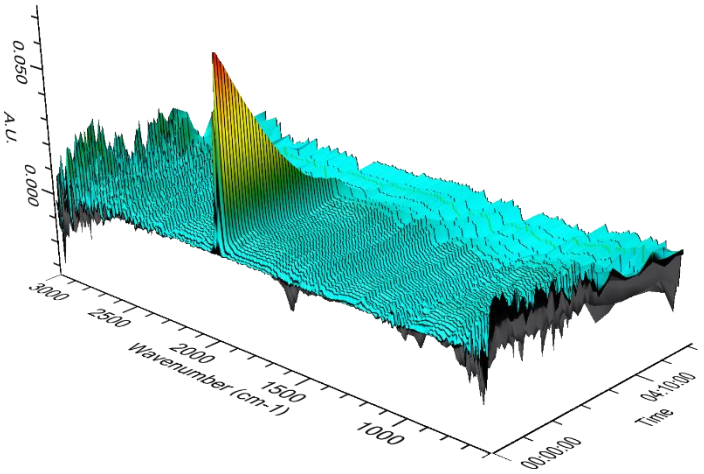

Figure 2.8: In situ IR spectrum as a function of time, illustrating the addition and subsequent removal of CO from toluene solution.

2.4.3 Study of the Bimetallic Rhodium Intermediate BM1

As mentioned in the introduction, one of the goals of this work was to unambiguously assign the peaks in the IR spectra to reaction intermediates along the cycloaddition pathway. One proposed method of making such assignments involves computing theoretical IR spectra for the intermediates that are believed to be in solution and then apply a vibrational scaling factor to match the computed vibrational frequencies to the experimental frequencies. As a solid state structure had already been obtained for **BM1** (see Figure 2.3), the idea was to use this structure as the starting geometry in a calculation of the corresponding theoretical IR spectrum. Thus, **BM1** was synthesized and

studied by IR so that a comparison could be made between the experimental and theoretical IR spectra and so that the scaling factors found in the literature could be tested.

With the addition of rhodium dimer catalyst to toluene solution, four peaks were observed at 2003, 2032, 2077, and 2088 cm^{-1} in the carbonyl region (see Table 2.2). The 2077 cm^{-1} peak was resolved through second derivative analysis. The addition of 1 equiv. of VCP and excess CO to this solution did not change the IR spectrum.

Table 2.2: In situ IR trial of the formation of **BM1**.

Note	**Wavenumber (cm^{-1})**			
Rh cat Addition	2003	2032	2077	2088
VCP Addition	2006	2032	2077	2088
CO Addition	2003	2032	2077	2088
Stir 10 mins	2003	2032	2077	2088

Figure 2.9 illustrates the usefulness (and major downfall) of this technique, as a hidden shoulder peak is now revealed but the signal-to-noise ratio has significantly decreased (note the different scales of the y-axis).

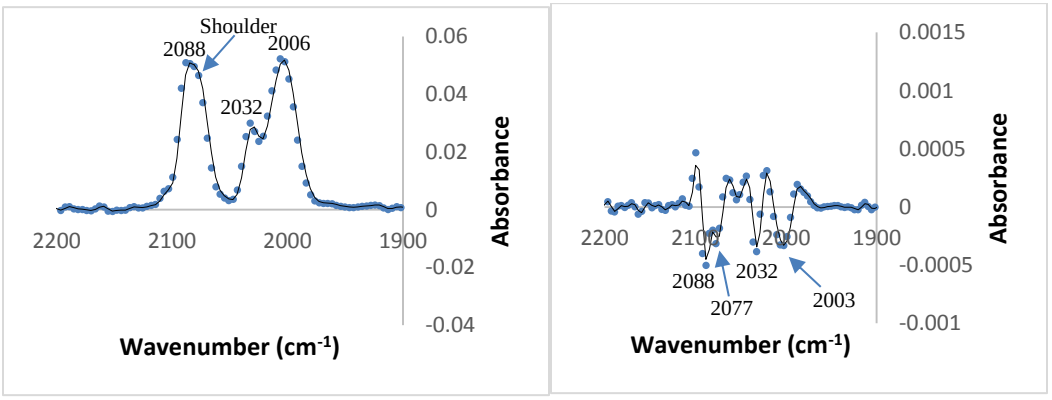

Figure 2.9: In situ IR spectra of the Rh dimer catalyst before second derivative analysis (left) and after (right) for the trial involving the formation of the bimetallic Rh intermediate **BM1**.

The change of wavenumber from 2006 cm^{-1} to 2003 cm^{-1} is not deemed significant, as the resolution of the spectrometer is only 4 cm^{-1}.

The IR spectrum for the rhodium catalyst during the **BM1** synthesis trial did not match that obtained when studying the [5+1+2+1] cycloaddition reaction. A possible explanation is that different concentrations of the rhodium catalyst were used in the two trials. When studying the [5+1+2+1] cycloaddition reaction, 0.5 mg of catalyst was added to 1.5 mL of solvent, whereas the study of **BM1** used 7.7 mg of catalyst in 1.5 mL of solvent. It is important to note that in order for the rhodium dimer catalyst to react with VCP, CO ligands must dissociate. Therefore, higher concentrations of catalyst could potentially result in greater concentrations of free CO in solution. However, the peak observed at 2032 cm^{-1} (see Table 2.2) does not match that of free CO.

Additionally, it is possible that the same species are present in both cases, but the higher concentration allows lower intensity peaks to be observed. If this were the case, one would expect the two new peaks at 2032 and 2088 cm^{-1} to have lower intensities than the two peaks that both spectra have in common. Referencing Figure 2.9, it appears that one of the new peaks at 2088 cm^{-1} is just as intense as one of the original peaks at 2006 cm^{-1}, thus ruling out this explanation.

The IR spectra of this trial involving the formation of **BM1** also did not meet expectations due to the lack of a carbonyl peak in the 1700-1800 cm^{-1} region of the spectrum after the addition of CO to the solution containing catalyst and VCP. **BM1** has an inserted carbonyl ligand (see Figure 2.3), and this CO stretch is expected to appear in this region. The bimetallic species might have been formed, but its concentration was

perhaps too low to observe the IR stretch of the inserted carbonyl ligand. Another possible explanation is that the bimetallic species was not being formed in this trial despite following the Mbaezue procedure.

To test the reproducibility of the in situ IR spectrometer, this solution was again tested at a later time and a ^{1}H NMR spectrum was also obtained. The in situ IR spectra of the two trials of the same solution appeared to be the same, although the signal-to-noise ratio of the second trial was too poor to be certain. The ^{1}H NMR strongly suggested that the species in solution is the same as that synthesized by Mbaezue when VCP was reacted with 1 equiv. of $[Rh(CO)_2Cl]_2$ with excess CO, with minor differences in the ^{1}H spectrum being attributed to the use of a different batch of VCP and a different NMR solvent. Overall, these observations suggest that either the concentration of **BM1** is too low for the stretch of the inserted carbonyl ligand to be seen, or the solid state structure of **BM1** is not representative of the species present in solution. In other words, perhaps the bimetallic species that slowly crystallizes out of solution is not the species that was originally observed by ^{1}H NMR in solution.

2.5 Computed IR Frequencies

The solid state structure of **BM1** was used as the starting geometry in calculations to determine the corresponding theoretical IR spectrum. As previously stated, these theoretical IR peaks were to then be compared to the experimental spectrum of the same species. The vibrational scaling factors for Rh(I) carbonyl compounds reported by Kohls and Stein were obtained from calculations using BP86 and B3LYP functionals with the def2-TZVP basis set.[66] Using Spartan ’16, calculations were performed using BPW91 and

B3LYP functionals using the def2-TZVP basis set. The BPW91 functional was used in place of BP86 since the BP86 functional was unavailable on Spartan ’16. Knowing that solvents can affect the peak positions of the IR spectrum, solvation calculations were included in the IR spectrum calculations. The C-PCM solvation method was used, as it is not parameterized for any particular atom and is available for any atom as long as an atomic radius is provided to generate the solvation cavity. In particular, to construct the cavity in the PCM solvation calculation, a Bondi Radius (increased by 20%) is used. These Bondi Radii are van der Waals radii originally proposed by Bondi[69] in 1964 and later verified by Rowland and Taylor[70] in 1996. The equilibrium geometry calculations performed at BPW91/def2-TZVP and B3LYP/def2-TZVP levels of theory failed to converge to a minimum, with many imaginary frequencies being observed (noting that at a minimum, no imaginary frequencies should be observed). Since these calculations failed to converge to a minimum, a frequency calculation was performed using the ωB97X-D functional and 6-31G* basis set, including C-PCM solvation. This calculation properly converged to a minimum and generated theoretical IR frequencies at 1839, 2142, 2189, and 2207 cm^{-1} for **BM1**. The peak at 1839 cm^{-1} is due to the inserted carbonyl ligand. As stated in section 2.4.3, this peak does not appear in the experimental spectrum, as there are four peaks for this bimetallic species at 2003, 2032, 2077, and 2088 cm^{-1} (see Table 2.2). The theoretical peaks at 2142, 2189, and 2207 cm^{-1} roughly correspond to this range. There appears to be two problems with the theoretical spectrum in comparison to the experimental spectrum. Firstly, the experimental spectrum has an extra peak in the 2000 cm^{-1} range that the theoretical spectrum does not. Inserted carbonyls typically have stretches in the 1600-1800 cm^{-1} range. However, it is possible that this experimental stretch at 2003 cm^{-1} is from the

inserted carbonyl. Secondly, these theoretical peaks differ significantly from the experimental peaks, and a vibrational scaling factor for rhodium carbonyl compounds using ωB97X-D/6-31G* calculations could not be found in the literature. Making a rough assignment of the experimental peak at 2003 cm^{-1} to free CO (and assuming the other free CO peak at 2021 cm^{-1} is simply buried beneath the 2032 cm^{-1} peak and is not being resolved by second derivative analysis), the other three experimental peaks were compared to the theoretical peaks in the 2000 cm^{-1} range to see if they were systematically different.

$$\Delta\nu = \nu_{theoretical} - \nu_{experimental}$$

$$2142cm^{-1} - 2032cm^{-1} = 110cm^{-1}$$

$$2189cm^{-1} - 2077cm^{-1} = 112cm^{-1}$$

$$2207cm^{-1} - 2088cm^{-1} = 119cm^{-1}$$

From this simple comparison, it appears that there may be a systematic difference between the theoretical spectrum and experimental spectrum of the bimetallic rhodium intermediate since these wavenumber differences are roughly equal. However, a vibrational scaling factor cannot be derived from this one example. For instance, the scaling factors reported by Kohls and Stein were derived using a library of 45 experimentally characterized Rh(I) compounds from the literature.[66] Since a vibrational scaling factor for rhodium carbonyl compounds using ωB97X-D/6-31G* calculations could not be found in the literature, and a new vibrational scaling factor could not be derived due to time constraints, this avenue of research was deemed unfruitful. Thus, the unambiguous assignment of in situ IR peaks to proposed species in solution through the use of theoretically generated IR spectra was not successful.

Out of curiosity, the effect of applying the scaling factors derived by Kohls and Stein was subsequently investigated to see if these factors would correct the data despite them not being optimized for ωB97X-D/6-31G* calculations. These corrected theoretical peaks are illustrated in Table 2.3.

Table 2.3: Theoretical CO peaks for **BM1** after applying the scaling factors derived by Kohls and Stein.[66]

Functional	**Factor**	**Wavenumbers After Scaling (cm^{-1})**			
BP86	1.0074	1852	2158	2205	2223
B3LYP	0.9662	1777	2070	2115	2132

From Table 2.3, it is apparent that by applying these scaling factors, there is still a significant difference between the theoretical and experimental peak positions.

2.6 Computed Energies of the Monometallic and Bimetallic Cycloaddition Reaction Coordinate

Having isolated the bimetallic rhodium species of Figure 2.3, it was hypothesized that the previously proposed reaction coordinate for the [5+1+2+1] cycloaddition (and competing [5+1+1+2] pathway) may also proceed through a bimetallic mechanism to a certain extent. To test this idea, and to possibly gain further understanding as to why the reaction does not proceed from the bimetallic rhodium species, the energies of the monometallic and bimetallic reaction pathways were calculated. These pathways are illustrated in Scheme 2.1. TS 4b-5b, TS 6b.1-7b.1, and TS 6b.2-7b.2 of the bimetallic pathway are all lower in energy than the corresponding transition states (TS 5a-6a, TS 7a.1-8a.1, and TS 7a.2-8a.2) of the monometallic pathway.

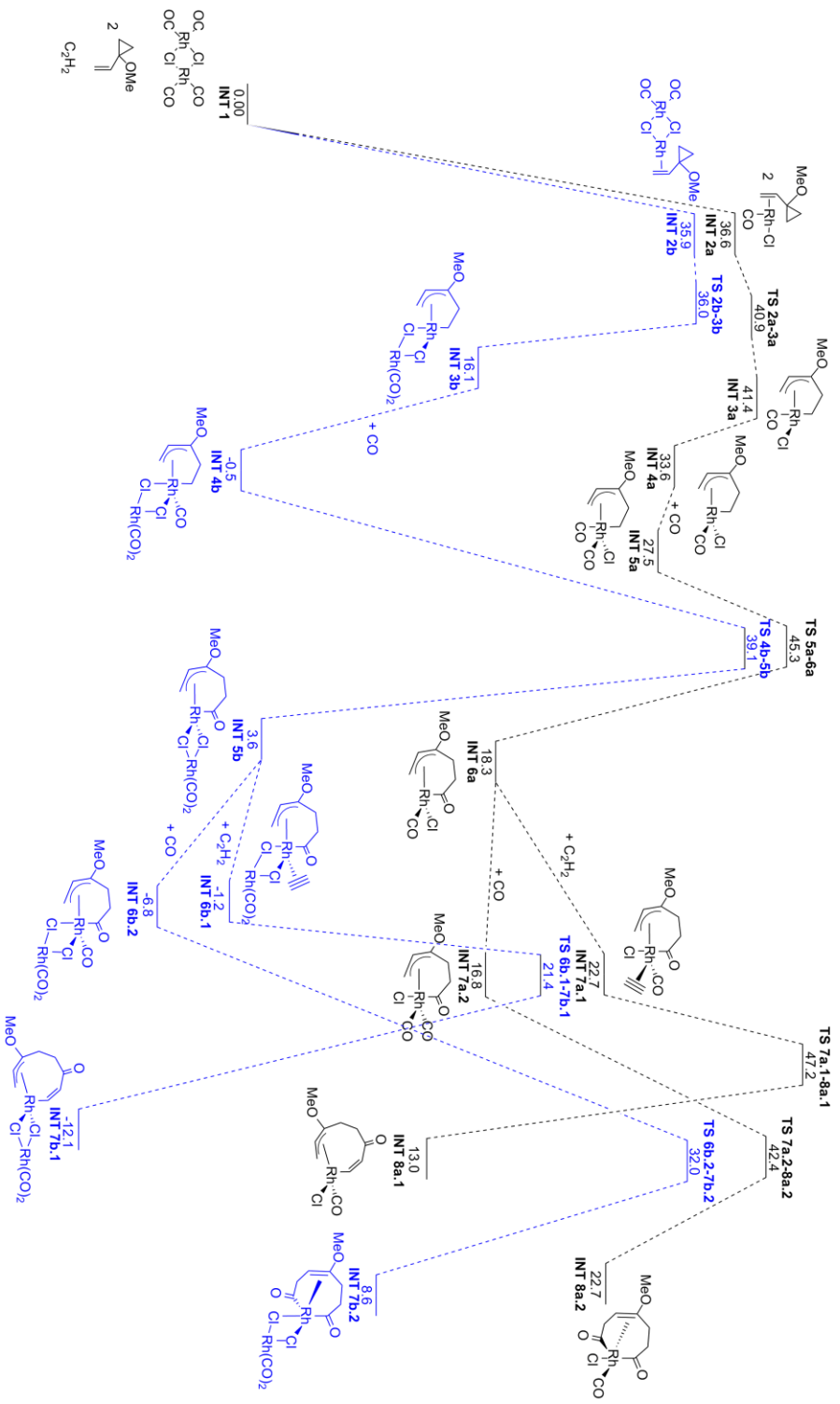

Scheme 2.2: Potential energy surface (kcal/mol) of the Rh catalyzed cycloaddition, including the [5+1+2] and [5+1+1] steps, as well as both the monometallic (black) and bimetallic (blue) pathways. Calculated at DFT ωB97X-D/6-31G* level of theory.

Additionally, all bimetallic intermediates are lower in energy than the monometallic intermediates. Thus, this scheme suggests that the bimetallic cycloaddition pathway is both kinetically and thermodynamically favourable. It is clear that this scheme does not agree with experimental results, as it has been previously shown that the reaction does not proceed past INT 6b.2 of the bimetallic pathway. This experimental result disagrees with what one might expect, considering that the coordinated CO ligand of INT 6b.2 is in the correct orientation (cis) for insertion. Furthermore, from this scheme, only 10.4 kcal/mol would be required for this "stuck" bimetallic intermediate to lose a CO ligand and coordinate an alkyne to proceed through the [5+1+2+1] pathway. However, this has also been shown not to occur experimentally, as the addition of alkyne to the solution of INT 6b.2 and CO did not allow the reaction to proceed.

There are several reasons as to why the computations of Scheme 2.1 may not reflect the experimental results. One reason is that the computations may need to be performed at a different basis set and may need to take into account solvent corrections. For instance, the previous computational study of this [5+1+2+1] cycloaddition reaction performed by Mbaezue and Ylijoki in 2017 used the SDD/6-31G* basis set (which more accurately models the electrons of the Rh atoms) and the polarizable continuum model[71] (PCM) for solvent corrections. It is important to note, however, that the computations of Scheme 2.1 were performed to quickly illustrate the relative energies of the monometallic and bimetallic pathways of the cycloaddition reaction and were not performed to give the most accurate, true to reality results. Another possible explanation for why the computations do not reflect the experimental results is that the proposed mechanism is not accurate, and that the reaction actually proceeds through a different, unknown mechanism. Finally, another

explanation is that the crystal of the rhodium bimetallic intermediate shown in Figure 2.3 may not be representative of the bulk solution whose ^{1}H NMR is shown in Figure 2.2. As such, it is possible that the inactive species that was previously assigned to INT 6b.2 may in fact be an entirely different species.

Chapter 3 – Summary & Conclusion

The vinylcyclopropane starting material was successfully prepared through modification of a previously reported 3-step synthetic method.[4] The [5+1+2+1] cycloaddition reaction reported by Wender et al.[2] was tested and confirmed to be reproducible in our laboratory, as crystals of the desired hydroxydihydroindanone cycloaddition product were obtained. In situ infrared spectroscopic studies of the cycloaddition reaction were performed. Although unsuccessful in identifying reaction intermediates of the cycloaddition pathway, second derivative analysis of the spectroscopic data proved successful in resolving overlapping CO peaks (albeit at the cost of decreased signal-to-noise ratio). Low concentrations of the rhodium catalyst are required for the reaction to proceed, but like the previous NMR studies conducted by Mbaezue, these concentrations were too low to properly observe the reaction intermediates spectroscopically. The IR frequency calculation (performed using the functional and basis set needed to apply the reported vibrational scaling factor) failed to converge to a minimum. As a result, experimentally obtained spectra of the reaction solution could not be compared to theoretical pure spectra of components believed to be in solution. Finally, a DFT investigation of the monometallic and bimetallic cycloaddition pathways suggested that the bimetallic pathway is both kinetically and thermodynamically favourable, which is inconsistent with previous experimental results.

Chapter 4 – Future Work

As this thesis has illustrated, in situ IR spectroscopy does not appear to be a fruitful avenue of investigation to determine the reaction intermediates along the [5+1+2+1] cycloaddition pathway due to poor signal. Although previous NMR studies have demonstrated that the reaction intermediates are too low in concentration to be observed, NMR spectroscopy still might prove valuable in determining kinetic information about the reaction, and thus, mechanistic information. For instance, it might be possible to use the acetylene proton of the alkyne as a reaction handle to determine its rate of consumption.

Further crystallization attempts should be made in order to isolate the second component of the two component rhodium intermediate mixture (as shown in the ^{1}H NMR of Figure 2.1). The technique of slow evaporation from toluene was used in this thesis, but perhaps other techniques such as slow cooling or solvent diffusion in combination with the use of other solvents might allow for the crystallization of this other, elusive species.

Finally, performing computations of the monometallic and bimetallic reaction pathways of the [5+1+2+1] cycloaddition reaction at ωB97X-D-SDD/6-31G* level of theory with PCM solvent corrections may result in energies that more accurately reflect previous experimental results.

Chapter 5 – Experimental

5.1 General Procedures

All preparations and in situ IR trials were performed on the benchtop and not under an inert atmosphere unless otherwise stated. Nitrogen (>99.998%) and carbon monoxide (>99%) were purchased from Praxair Inc. Anhydrous 2-methoxyethanol (99.8%), 1,3-butadiene (20 wt. % in toluene), copper (I) chloride (97%), acetyl chloride (98%), diiodomethane (99%), and 4-ethynylbiphenyl (97%) were purchased from Sigma-Aldrich and used without further purification, while NBS was purified via methods reported by Dauben and McCoy.[72] 20 mesh granular zinc was purchased from Fisher Chemical and was purified according to a procedure reported by Smith and Simmons.[67] (***Note:*** *This procedure by Smith and Simmons is for the formation of a zinc-copper couple. To simply purify the zinc, the step involving portions of 2% aqueous copper sulfate solution has been omitted*). The zinc was dried in a vacuum desiccator with P_2O_5 overnight and transferred into an MBRAUN glove box for long term storage. Chloroform-*d* (D: 99.8%) and toluene-d_8 (D: 99.5%) were both purchased from Cambridge Isotope Laboratories Inc. and used without further purification. Solvents were obtained from an MBRAUN solvent purification system except in the synthesis of VCP, where diethyl ether was used as purchased from Fisher Chemical. The concentration of organic solutions was carried out via a Buchi rotary evaporator connected to a tap for vacuum control. High-boiling solvents such as toluene were removed via a vacuum manifold, at a reduced pressure of 250-500 μTorr. Water soluble solvents such as 2-methoxyethanol were removed in the aqueous layer during liquid-liquid extractions.

5.2 General Spectroscopic and Characterization Techniques

The infrared spectrum of brominated intermediate **1** was obtained using an attenuated total reflectance (ATR) adapter on a Bruker Alpha Spectrometer. This data was processed using the OPUS 6.0 software suite. The in situ infrared spectra were obtained using a Mettler-Toledo ReactIR 15 spectrometer equipped with a silicon-tipped probe and were processed using iC.IR 4.3 software. Before each in situ IR experiment, an instrument calibration was performed and a reference spectrum of toluene was obtained. This toluene reference spectrum was then subtracted from all in situ IR spectra. Microsoft Office Excel 2013 was used to both plot these spectra and to perform second derivative analysis.

The NMR spectra were obtained using a Bruker Ultrashield 300 MHz NMR spectrometer with a 7.05 Tesla magnet. The NMR data was processed using both Bruker TOPSIN 4.0.3 and ACD/NMR Processor Academic Edition 12.01 software suites. ^{1}H and $^{13}C\{^{1}H\}$ spectra were referenced to tetramethylsilane (TMS).

High resolution mass spectrometry (positive mode) analysis of brominated intermediate **1** was performed on a Bruker microTOF Focus Mass Spectrometer by the method of atmospheric-pressure chemical ionization in acetonitrile. The HRMS data was collected by Xiao Feng of the Maritime Mass Spectrometry Laboratories at Dalhousie University in Halifax, Nova Scotia.

For computational and crystallographic details, see sections 5.9 and 5.10, respectively.

5.3 Synthesis of 1-(2-methoxyethoxy)-1-vinylcyclopropane (VCP)

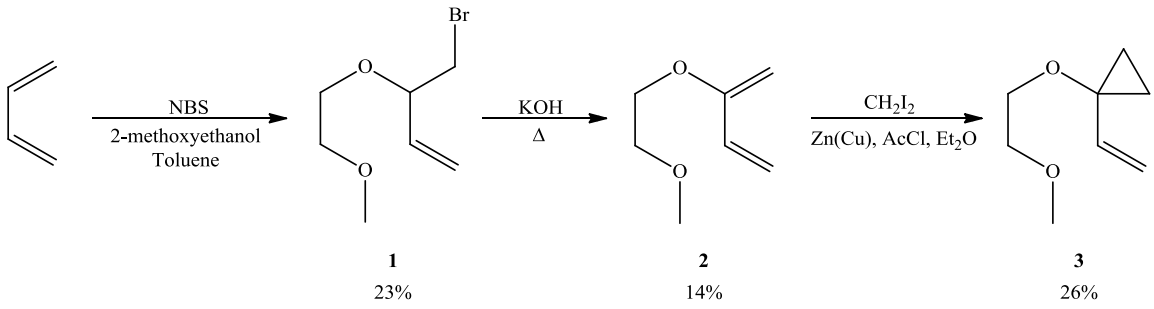

Scheme 2.1: Multistep sequence for the synthesis of VCP, including isolated yields.

5.3.1 Synthesis of Brominated Intermediate 1

White, fluffy crystals of purified N-bromosuccinimide (49.5 g, 278 mmol) were crushed using a mortar and pestle and added to 2-methoxyethanol (276 mL, 3500 mmol) in a 1L round-bottom flask. The flask was subsequently cooled to −78 ºC via a dry ice-acetone bath. Afterward, 124 mL of 20 wt. % 1,3-butadiene in toluene (20 g, 370 mmol of 1,3-butadiene) was added. This mixture was stirred overnight for 18 hours. The organic solution was then diluted with 200 mL of distilled water, resulting in a light yellow aqueous layer on the bottom of the flask with a yellow/brown organic layer resting on top. The aqueous layer was extracted with diethyl ether (3 × 150 mL) and washed with brine (4 × 150 mL) until no more white solids crashed out of solution. The combined organic layer was dried over $MgSO_4$ and then concentrated in vacuo until no more solvent condensed into the collection vessel. In order to remove the remaining solvent, the solution was evacuated at room temperature (250-500 μTorr) for ca. 5 hours. After that time, the flask was no longer cool from solvent evaporation and the yellow/brown brominated intermediate **1** was isolated. Yield = 13.5 g (23% based upon consumption of NBS).

Spectroscopic data is consistent with that found in the literature.[4] (***Note:*** *The spectroscopic data of brominated intermediate* ***1*** *presented in the appendix was obtained after column purification.*) ^{1}H (300 MHz, $CDCl_3$, ppm): 3.34-3.46 (m, 5H, –OC<u>H</u>$_3$, –C<u>H</u>$_2$OCH$_3$), 3.54-3.61 (m, 3H, –C<u>H</u>HBr, –OC<u>H</u>$_2$CH$_2$OCH$_3$), 3.66-3.74 (m, 1H, –C<u>H</u>HBr), 3.97 (q, 1H, $^{3}J_{HH}$ = 6.37 Hz, –OC<u>H</u>CH$_2$Br), 5.30-5.38 (m, 2H, –CH=C<u>H</u>$_2$), 5.74 (ddd, 1H, $^{3}J_{HH}$ = 17.30 Hz, 10.20 Hz, 7.13 Hz, –OCHC<u>H</u>=CH$_2$). ^{13}C{^{1}H} (75 MHz, $CDCl_3$, ppm): 34.55 (s, –O<u>C</u>H$_3$), 59.06 (s, –<u>C</u>H$_2$OCH$_3$), 68.47 (s, –<u>C</u>H$_2$Br), 71.93 (s, –O<u>C</u>H$_2$CH$_2$OCH$_3$), 81.00 (s, –O<u>C</u>HCH$_2$Br), 119.31 (s, –CH=<u>C</u>H$_2$), 135.79 (s, –<u>C</u>H=CH$_2$). IR (ATR, cm^{-1}): 3081 (w), 2983 (w), 2924 (w), 2876 (w), 2821 (w), 2247 (w), 1455 (w), 1421 (w), 1221 (w), 1199 (m), 1088 (vs), 1030 (m), 990 (m), 930 (m), 910 (m), 849 (w), 730 (vs), 700 (m), 677 (w), 647 (w). HRMS calcd. [m/z]: 230.9997, 232.9976; found [m/z]: 231.0001, 232.9979.

5.3.2 Synthesis of Diene 2

All of brominated intermediate **1** (13.5 g, 65 mmol) was placed in a 500 mL round-bottom flask which was fully submerged in ice. Crushed KOH (39.6 g, 706 mmol) was then added slowly. ***Caution!*** *It is important to add the KOH slowly due to the exothermic nature of the reaction.* Water (2.5 mL, 139 mmol) and 2-methoxyethanol (50 mL, 634 mmol) were subsequently added. The flask was fitted with a condenser and heated to 72 ºC for 3 hours. During the heating, the solution gradually changed colour from yellow to dark brown. After heating for 3 hours, the solution was allowed to cool to room temperature and was then extracted with pentane (3 × 150 mL). This organic solution was washed with brine (150 mL), dried over $MgSO_4$, and filtered to obtain a clear, light yellow solution. The pentane was subsequently removed by fractional distillation at 60 ºC. The distillation was stopped after ca. 1 hour, when the solution had ceased to boil. Afterward, the solution was

vacuum distilled (see section **5.4**) to afford clear and colourless diene **2**. Yield = 1.2 g (14 % based upon consumption of brominated intermediate **1**). Spectroscopic data is consistent with that found in the literature.[4,68] ^{1}H (300 MHz, $CDCl_3$, ppm): 3.42 (s, 3H, –OC<u>H</u>$_3$), 3.69-3.72 (m, 2H, –OCH$_2$C<u>H</u>$_2$OCH$_3$), 3.89-3.92 (m, 2H, –OC<u>H</u>$_2$CH$_2$OCH$_3$), 4.15 (s, 2H, –OC=C<u>H</u>$_2$), 5.10 (d, 1H, $^3J_{HH}$ = 10.90 Hz, –CH=C<u>H</u>H *trans* to R group), 5.61 (dd, 1H, $^2J_{HH}$ = 1.45 Hz; $^3J_{HH}$ = 17.25 Hz, –CH=CH<u>H</u> *cis* to R group), 6.15 (dd, 1H, $^3J_{HH}$ = 10.85 Hz, 17.25 Hz, –C<u>H</u>=CH$_2$).

5.3.3 Synthesis of VCP 3

Purified zinc (1.4346 g, 21.9 mmol) and copper (I) chloride (0.2208 g, 2.2 mmol) were added to a 50 mL round-bottom flask and suspended in 5 mL of diethyl ether. Diiodomethane (0.4285 mL, 5.3 mmol) and acetyl chloride (36 μL, 0.5 mmol) were subsequently added to the flask. This light grey/tan suspension was then set to reflux for 40 minutes. Over this time, the suspension gradually changed colour to a very dark grey. Afterward, diene **2** (0.6817 g, 5.3 mmol) was added dropwise down the condenser and washed down with ca. 1 mL of diethyl ether. The reaction was monitored by TLC every hour (20% EtOAc 80% hexanes, followed by the use of a UV lamp and then iodine vapour staining to observe spots). (***Note:*** *Two major spots appear roughly halfway up the TLC plate in close proximity to one another. The spot with R_f = 0.56 was both UV and I_2 active and was assigned to the starting diene **2**. The spot with R_f = 0.46 was only I_2 active and was assigned to VCP **3**.*) The reaction was complete 7 hours after the addition of diene **2**. The flask was allowed to cool to room temperature and the solution was decanted into a 150 mL Erlenmeyer flask. The solids in the reaction flask were rinsed with diethyl ether (3 × 150 mL) and decanted into the Erlenmeyer flask. The combined organic solution was

cooled to 0 ºC via an ice bath and saturated NH_4Cl aqueous solution (16 mL) was added. The aqueous layer was then extracted with pentane (3 × 30 mL). Afterward, this organic solution was washed with 1 M NaOH (3 × 30 mL) followed by brine (30 mL) and then dried over $MgSO_4$ and concentrated in vacuo under minimal pressure to afford clear and colourless VCP **3**. Yield = 0.1983 g (26% based upon consumption of diene **2**). Spectroscopic data is consistent with that found in the literature.[4,68] ^1H (300 MHz, $CDCl_3$, ppm): 0.69-0.73 (m, 2H, –CC<u>H</u>HC<u>H</u>H– same face of the cyclopropane ring), 1.04-1.08 (m, 2H, –CCH<u>H</u>CH<u>H</u>– same face of the cyclopropane ring), 3.38 (s, 3H, –OC<u>H</u>$_3$), 3.50-3.53 (m, 2H, –OCH$_2$C<u>H</u>$_2$OCH$_3$), 3.61-3.64 (m, 2H, –OC<u>H</u>$_2$CH$_2$OCH$_3$), 5.07 (dd, 1H, $^2J_{HH}$ = 1.45 Hz; $^3J_{HH}$ = 10.75 Hz, –CH=C<u>H</u>H *trans* to R group), 5.21 (dd, 1H, $^2J_{HH}$ = 1.45 Hz; $^3J_{HH}$ = 17.25 Hz, –CH=CH<u>H</u> *cis* to R group), 5.64 (dd, 1H, $^3J_{HH}$ = 10.70 Hz, 17.30 Hz, –C<u>H</u>=CH$_2$).

5.4 Vacuum Distillation of Diene 2

Copper wire was passed through the outlet opening of a cold trap, and wound around the outer surface of the inlet tube. This tube was inserted into a pre-weighed vial and secured using the free end of the copper wire. The secured inlet tube and vial were inserted into the receiving tube of the trap, which was subsequently sealed with grease. The inlet opening of the trap was connected via vacuum resistant tubing to another vial containing a stir bar and crude diene **2**. The outlet opening of the trap was connected to a second trap immersed in liquid nitrogen. The second trap was then connected to the vacuum line of an Edwards pump. Both traps were evacuated at 250-500 μTorr for ca. 20 minutes. Afterwards, the vial was opened to vacuum for ca. 2 minutes while stirring the contents. The first trap (directly connected to the vial) was immersed in liquid nitrogen and the vial

was heated to 67 ºC while stirring. After boiling ceased in the vial, the system was disassembled and the clean diene **2** was obtained from the vial connected to the first trap.

5.5 Test of the [5+1+2+1] Cycloaddition Reaction

VCP (0.0171 g, 0.1203 mmol), $[Rh(CO)_2Cl]_2$ (0.0006 g, 0.0015 mmol), and 4-ethynylbiphenyl (0.0107 g, 0.0600 mmol) were weighed out in separate vials in the glovebox. VCP was then dissolved in 300 μL of toluene-d_8 and added to the vial with the rhodium catalyst. The alkyne was also dissolved in 300 μL of deuterated toluene and was added to the VCP and rhodium catalyst solution. The combined solution was added to an NMR tube, which was then capped with a rubber septum and removed from the glovebox. A thin, long, stainless steel needle (attached to a CO tank) was used to pierce the rubber septum of the NMR tube; simultaneously, a 21 G needle was used to pierce another hole in the septum for venting purposes. The headspace of the NMR tube was then purged with CO for 15 minutes, with the needle close to the surface of the solution. Afterward, the septum pierced with needles was quickly removed and a new rubber septum was quickly placed on the NMR tube and sealed with parafilm to ensure that the CO atmosphere was maintained in the tube. Heating the solution in an oil bath at 60 ºC for ca. 40 hours resulted in a colour change from light orange/red to very dark brown. Clear, pale yellow/brown, rod-like crystals precipitated from solution.

5.6 Crystallization Attempt of Rhodium Intermediates

$[Rh(CO)_2Cl]_2$ (0.0261 g, 0.0671 mmol) was dissolved in 700 μL of toluene-d_8 and added to a vial containing 1 equiv. of VCP (0.0095 g, 0.0668 mmol) in the glovebox. This solution was then transferred into an NMR tube, which was then sealed and taken out of

the glovebox for a ^{1}H NMR experiment. After the experiment, the NMR tube was brought back into the glovebox, the cap of the tube was cracked open slightly, and the solution was left to slowly evaporate under the inert nitrogen atmosphere. Bright red, needle-like crystals were obtained from dark brown oil 14 weeks later.

5.7 In Situ Infrared Spectroscopic Studies

5.7.1 Study of the [5+1+2+1] Cycloaddition

VCP (0.0144 g, 0.1013 mmol), $[Rh(CO)_2Cl]_2$ (0.0005 g, 0.0013 mmol), and 4-ethynylbiphenyl (0.0086 g, 0.0483 mmol) were weighed out in separate vials in the glovebox and dissolved in 5 drops of toluene each. The calibrated ReactIR probe was then placed into a 100 mL three-neck round-bottom flask containing stirring toluene (1.5 mL) with the instrument being set to a total sampling period of 3 days with a sampling interval of 2 minutes (the minimum interval that could be selected for a 3 day experiment period). The prepared rhodium catalyst, VCP, and 4-ethynylbiphenyl solutions were then taken outside of the glovebox and injected (in that order) into the stirring solution of toluene, ensuring that at least a couple scans were obtained between each subsequent addition. Once these solutions were added, CO was bubbled into solution using a long, thin, stainless steel needle for ca. 5 minutes and then sprayed just above the solution surface for another 30 minutes. The round-bottom flask was sealed with septa and parafilm except for the CO needle in and the venting needle out. After removal of the needles and after greasing and parafilming the newly formed holes, the scanning interval was lengthened to 5 minutes and the reaction vessel was heated to 60 ºC for 32 hours before going dry.

5.7.2 Study of the [5+1+2+1] Cycloaddition Reaction with N_2 Sparging

VCP (0.0140 g, 0.0985 mmol), $[Rh(CO)_2Cl]_2$ (0.0005 g, 0.0013 mmol), and 4-ethynylbiphenyl (0.0087 g, 0.0488 mmol) were weighed out in separate vials in the glovebox and dissolved in 10 drops of toluene each. The calibrated ReactIR probe was then placed into a 100 mL three-neck round-bottom flask containing stirring toluene (1.5 mL), with the instrument being set to a total sampling period of 3 days with a sampling interval of 2 minutes. The prepared rhodium catalyst, VCP, and 4-ethynylbiphenyl solutions were then taken outside of the glovebox and injected (in that order) into the stirring solution of toluene, ensuring that 2 scans were obtained between each subsequent addition. CO was bubbled into solution for 5 minutes. Afterward, N_2 was then sparged through solution for 40 minutes, followed by bubbling CO for 10 minutes with CO being sprayed on the solution surface for an additional 10 minutes. The reaction vessel was then sealed and heated to 60 ºC, with the scanning interval being changed to 5 minutes. A second N_2 sparging cycle was performed ca. 21 hours after the first sparging cycle. During this second cycle, N_2 was bubbled through solution for 30 minutes, followed by CO being bubbled for 15 minutes with an additional 10 minutes of CO being sprayed in the flask headspace. Subsequently, the reaction vessel was sealed again and the reaction continued to proceed at 60 ºC for ca. 15 hours.

5.7.3 Study of the Solubility of CO in Toluene

The calibrated ReactIR probe was first placed into ca. 2 mL of stirring toluene in a 100 mL three-neck round-bottom flask and set to 1 minute scanning intervals. Using a long, thin needle, CO was then bubbled into solution for ca. 5 minutes. After this, N_2 was bubbled

into solution overnight. The scanning interval was lengthened to 5 minutes once the asymptotic nature of the CO peak decrease was observed.

5.7.4 Study of the Bimetallic Rhodium Species

The calibrated ReactIR probe was first placed into 1.5 mL of stirring toluene in a 100 mL three-neck round-bottom flask and set to 15 second scanning intervals. VCP (0.0032 g, 0.0225 mmol) and $[Rh(CO)_2Cl]_2$ (0.0077 g, 0.0198 mmol) were weighed into separate vials in the glovebox and each dissolved in 100 μL of toluene. These vials were then taken outside of the glovebox and then injected into the toluene solution (rhodium catalyst solution was first injected, followed by the VCP solution). Several scans were obtained between these additions. After this, CO was bubbled through solution for ca. 10 minutes. Afterward, the reaction was left to stir for ca. 10 minutes.

5.8 Second Derivative Analysis Details

A series of data points was obtained by the ReactIR ((x,y) = (wavenumber, absorbance)), which was then fitted with a moving average trendline. As these points could not be appropriately fitted to a polynomial function, finding the second derivative became slightly more involved. The derivatives were calculated by taking the difference in absorbance between two closely spaced wavenumbers and dividing by the difference in wavenumber for all wavenumbers. This can be expressed by the following equation:

$$D_{\nu+(\Delta\nu/2)} = \frac{(A_{\nu+\Delta\nu} - A_{\nu})}{\Delta\nu} \quad (5.1)$$

The infrared spectrum can be seen as absorbance as a function of wavenumber, or A(ν). Another notation for this derivative, which was used to calculate both the first and second derivative, is shown by the following equations:

$$A'(\nu) = \frac{A(\nu + \Delta\nu) - A(\nu - \Delta\nu)}{(\nu + \Delta\nu) - (\nu - \Delta\nu)} \quad (5.2)$$

$$= \frac{A(\nu + \Delta\nu) - A(\nu - \Delta\nu)}{2\Delta\nu} \quad (5.3)$$

The resolution of the instrument is 4 cm^{-1}. Therefore, that is the $\Delta\nu$ value that was used to calculate the derivative.

5.9 Computational Details

Calculations for the monometallic and bimetallic reaction pathways were performed using the Spartan '14 software package,[73] unless otherwise stated. For the monometallic reaction pathway, (x, y, z) coordinates were obtained from the previous computational study of this [5+1+2+1] cycloaddition reaction and were input into Spartan to give the initial geometries. DFT single point energy calculations were then performed at the ωB97X-D[74] level of theory using the 6-31G* basis set. Calculations of the equilibrium geometry were then performed at the same level of theory, using the same basis set.

For the bimetallic reaction pathway, structures were first drawn using the graphical interface, followed by computing the equilibrium geometry at the semi-empirical PM3[75] level of theory. The lowest energy conformations were then used as the initial geometries for DFT calculations of the equilibrium geometries at B3LYP[76,77], and, subsequently, ωB97X-D levels of theory using the 6-31G* basis set. Vibrational frequency calculations

were performed on all intermediates to verify that the geometries were in fact at a minimum (no imaginary frequencies present). These frequency calculations were also performed on all transition states to verify that the geometries were at a maximum (only one imaginary frequency present). For computational efficiency, the 2-methoxyethoxy group of the VCP was replaced with a methoxy group. To account for the entropy overestimation of the gas-phase calculations, the solution Gibbs energy was corrected by applying free volume theory with the following equation, where *m* is the molecularity of the process[78–82]:

$$\Delta G^{\circ}_{sol} = \Delta G^{\circ}_{gas} - RT((1-m) + \ln(10^{2m-2}m)) \quad (5.4)$$

This equation can be greatly simplified to give Eqn. 5.5, where X = 2.6, 5.0, and 7.3 kcal/mol for bi-, tri-, and tetramolecular processes, respectively:

$$\Delta G^{\circ}_{sol} = \Delta G^{\circ}_{gas} - X \quad (5.5)$$

Theoretical infrared spectra for the optimized structures were generated using Spartan '16 at the ωB97X-D level of theory using the 6-31G* basis set, including C-PCM solvation[71] (Solvent = Toluene) and using a 2.0 Å radius for each rhodium atom.

5.10 X-ray Crystallographic Details

5.10.1 General Details

All X-ray crystallographic analyses were performed by Dr. Katherine Robertson at Saint Mary's University, and all crystallographic diagrams presented within were prepared using Mercury CSD 3.7.[83]

The crystal chosen was attached to the tip of a 200 μm MicroLoop with paratone-N oil. Measurements were made on a Bruker APEXII CCD equipped diffractometer (30 mA, 50 kV) using monochromated Mo Kα radiation (λ = 0.71073 Å) at 125 K.[84] The initial orientation and unit cell were indexed using a least-squares analysis of a random set of reflections collected from three series of 0.5° ω-scans, 10 seconds per frame and 12 frames per series, that were well distributed in reciprocal space. For data collection, four ω-scan frame series were collected with 0.5° wide scans (45, 60, and 15 second frames for the bimetallic rhodium intermediate, the hydroxydihydroindanone cycloaddition product, and the rhodium dimer catalyst, respectively, with 366 frames per series) at varying φ angles (φ = 0°, 90°, 180°, 270°). The crystal to detector distance was set to 6 cm and a complete sphere of data was collected. Cell refinement and data reduction were performed with the Bruker SAINT software,[85] which corrects for beam inhomogeneity, possible crystal decay, Lorentz and polarisation effects. A multi-scan absorption correction was applied (SADABS).[86] The structure was solved using SHELXT-2014[87,88] and was refined using a full-matrix least-squares method on F^2 with SHELXL-2014[87,89] for the bimetallic rhodium intermediate and SHELXL-2018[87,89] for the hydroxydihydroindanone cycloaddition product and the rhodium dimer catalyst. The non-hydrogen atoms were refined anisotropically. Hydrogen atoms bonded to carbon were included at geometrically idealized positions and were not refined. The isotropic thermal parameters of the hydrogen atoms were fixed at $1.2U_{eq}$ of the parent carbon atom or $1.5U_{eq}$ for methyl hydrogens. However, there were no hydrogen atoms present in the rhodium dimer catalyst structure. All diagrams were prepared using the program Mercury CSD 3.7.

5.10.2 Refinement Details

During the refinement process of the bimetallic rhodium intermediate, two hydrogen atoms were placed in geometrical positions on C(1). However, these positions proved to be less than satisfactory and two Fourier peaks remained close to C(1). The riding hydrogens were removed and the positions of the Fourier peaks used to introduce two hydrogens into the refinement. They were allowed to refine without restraints and with isotropic thermal parameters.

During the refinement of the hydroxydihydroindanone cycloaddition product, one reflection (-8 1 3) showed poor agreement in the final refinement and was removed from the data set. The routine TwinRotMax implemented in Platon[90] indicated that there was a minor twin component present in the crystal. The twin law, TWIN -1 0 0 0 -1 0 0.668 0 1, was added to the refinement and the BASF scale factor refined to 0.0034(7). Inclusion of the twin law did improve the statistics of the refinement slightly.

Finally, all refinements for the rhodium dimer catalyst structure were unremarkable.

References

(1) Lautens, M.; Klute, W.; Tam, W. *Chem. Rev.* **1996**, *96*, 49–92.

(2) Wender, P. A.; Gamber, G. G.; Hubbard, R. D.; Pham, S. M.; Zhang, L. *J. Am. Chem. Soc.* **2005**, *127*, 2836–2837.

(3) Mbaezue, I. I.; Ylijoki, K. E. O. *Organometallics* **2017**, *36*, 2832–2842.

(4) Mbaezue, I. I. An Investigation of the Mechanism of the Rhodium-Catalyzed [5 + 1 + 2 + 1] Cycloaddition Reaction of Vinylcyclopropanes, Terminal Alkynes and Carbon- Monoxide, Saint Mary's University, Halifax, NS, 2017.

(5) Park, C. H.; Siomboing, X.; Yous, S.; Gressier, B.; Luyckx, M.; Chavatte, P. *Eur. J. Med. Chem.* **2002**, *37*, 461–468.

(6) Ballinger, A.; Smith, G. *Expert Opin. Pharmacother.* **2001**, *2*, 31–40.

(7) Fu, J. Y.; Masferrer, J. L.; Seibert, K.; Raz, A.; Needleman, P. *J. Biol. Chem.* **1990**, *265*, 16737–16740.

(8) Subbaramaiah, K.; Zakim, D.; Weksler, B. B.; Dannenberg, A. J. *Proc. Soc. Exp. Biol. Med.* **1997**, *216*, 201–210.

(9) Hsu, A. L.; Ching, T. T.; Wang, D. S.; Song, X.; Rangnekar, V. M.; Chen, C. S. *J. Biol. Chem.* **2000**, *275*, 11397–11403.

(10) Pasinetti, G. M. *J. Neurosci. Res.* **1998**, *54*, 1–6.

(11) Hull, M.; Lieb, K.; Fiebich, B. L. *Expert Opin. Investig. Drugs* **2000**, *9*, 671–683.

(12) Ahn, J. H.; Shin, M. S.; Jung, S. H.; Kang, S. K.; Kim, K. R.; Rhee, S. D.; Jung, W. H.; Yang, S. D.; Kim, S. J.; Woo, J. R.; et al. *J. Med. Chem.* **2006**, *49*, 4781–4784.

(13) Willson, T. M.; Brown, P. J.; Sternbach, D. D.; Henke, B. R. *J. Med. Chem.* **2000**, *43*, 527–550.

(14) Picard, F.; Auwerx, J. *Annu. Rev. Nutr.* **2002**, *22*, 167–197.

(15) Demer, L. L. *Circ. Res.* **2002**, *90*, 241–243.

(16) International Diabetes Federation. IDF Diabetes Atlas. 7th edition http://www.diabetesatlas.org/ (accessed Oct 6, 2016).

(17) Morrell, A.; Placzek, M.; Parmley, S.; Grella, B.; Antony, S.; Pommier, Y.; Cushman, M. *J. Med. Chem.* **2007**, *50*, 4388–4404.

(18) Kohn, K. W.; Pommier, Y. *Ann. N. Y. Acad. Sci.* **2000**, *922*, 11–26.

(19) Takimoto, C. H.; Wright, J.; Arbuck, S. G. *Biochim. Biophys. Acta - Gene Struct. Expr.* **1998**, *1400*, 107–119.

(20) Oberlies, N. H.; Kroll, D. J. *J. Nat. Prod.* **2004**, *67*, 129–135.

(21) Pommier, Y.; Pourquier, P.; Fan, Y.; Strumberg, D. *Biochim. Biophys. Acta - Gene Struct. Expr.* **1998**, *1400*, 83–106.

(22) Thomas, C. J.; Rahier, N. J.; Hecht, S. M. *Bioorganic Med. Chem.* **2004**, *12*, 1585–1604.

(23) Witulski, B. *Angew. Chemie Int. Ed.* **2015**, *54*, 8030–8031.

(24) Heaton, B. *Mechanisms in Homogeneous Catalysis. A Spectroscopic Approach.*; Wiley-VCH: Weinheim, Germany, 2005.

(25) Forster, D. *J. Am. Chem. Soc.* **1976**, *98*, 846–848.

(26) Roth, J. F.; Craddock, J. H.; Hershman, A.; Paulik, F. E. *Chem. Technol.* **1971**, 600.

(27) Schrod, M.; Luft, G.; Grobe, J. *J. Mol. Catal.* **1983**, *22*, 169–178.

(28) Marr, A. C.; Lightfoot, P.; Ditzel, E. J.; Poole, A. D.; Schwarz, G. P.; Foster, D. F.; Cole-Hamilton, D. J. *Inorg. Chem. Commun.* **2000**, *3*, 617–619.

(29) Kang, J. W.; Maitlis, P. M. *J. Organomet. Chem.* **1971**, *26*, 393–399.

(30) Kang, J. W.; Moseley, K.; Maitiis, P. M. *J. Am. Chem. Soc.* **1969**, *91*, 5970–5977.

(31) Fontaine, M.; Castanet, Y.; Mortreux, A.; Petit, F. *J. Catal.* **1997**, *167*, 324–336.

(32) Forster, D. *Inorg. Chem.* **1969**, *8*, 2556–2558.

(33) Daly, J. J.; Sanz, F.; Forster, D. *J. Am. Chem. Soc.* **1975**, *97*, 2551–2553.

(34) Baker, E. C.; Hendriksen, D. E.; Eisenberg, R. *J. Am. Chem. Soc.* **1980**, *102*, 1020–1027.

(35) Vallarino, L. M. *Inorg. Chem.* **1965**, *4*, 161–165.

(36) Garland, M. *Organometallics* **1993**, *12*, 535–543.

(37) Garland, M.; Bor, G. *Inorg. Chem.* **1989**, *28*, 410–413.

(38) Marko, L.; Bor, G.; Almasy, G.; Szabo, P. *Brennst.-Chem.* **1963**, *44*, 184.

(39) Whyman, R. *J. Organomet. Chem.* **1974**, *66*, 23–25.

(40) Whyman, R. *J. Organomet. Chem.* **1974**, *81*, 97–106.

(41) Ford, P. C.; Massick, S. *Coord. Chem. Rev.* **2002**, *226*, 39–49.

(42) Simpson, M. B.; Poliakoff, M.; Turner, J. J.; Maier, W. B.; Mc Laughlin, J. G. *J. Chem. Soc. Chem. Commun.* **1983**, 22, 1355–1357.

(43) Perutz, R. N.; Turner, J. J. *J. Am. Chem. Soc.* **1975**, *97*, 4791–4800.

(44) Maier II, W. B.; Poliakoff, M.; Simpson, M. B.; Turner, J. J. *J. Chem. Soc. Chem. Commun.* **1980**, 587–589.

(45) Turner, J. J.; Simpson, M. B.; Poliakoff, M.; Maier, W. B.; Graham, M. A. *Inorg. Chem.* **1983**, *22*, 911–920.

(46) Weiller, B. H. *J. Am. Chem. Soc.* **1992**, *114*, 10910–10915.

(47) Sun, X. Z.; George, M. W.; Kazarian, S. G.; Nikiforov, S. M.; Poliakoff, M. *J. Am. Chem. Soc.* **1996**, *118*, 10525–10532.

(48) Massick, S. M.; Rabor, J. G.; Elbers, S.; Marhenke, J.; Bernhard, S.; Schoonover, J. R.; Ford, P. C. *Inorg. Chem.* **2000**, *39*, 3098–3106.

(49) Massick, S. M.; Buttner, T.; Ford, P. C. *Inorg. Chem.* **2003**, *42*, 575–580.

(50) Boese, W. T.; Ford, P. C. *J. Am. Chem. Soc.* **1995**, *117*, 8381–8391.

(51) Horvath, I. T.; Millar, J. M. *Chem. Rev.* **1991**, *91*, 1339–1351.

(52) Heaton, B. T.; Jonas, J.; Eguchi, T.; Hoffman, G. A. *J. Chem. Soc. Chem. Commun.* **1981**, 331–332.

(53) Dombek, H. D. *J. Chem. Educ.* **1986**, *63*, 210–212.

(54) Fumagalli, A.; Koetzle, T. F.; Takusagawa, F.; Chini, P.; Martinengo, S.; Heaton, B. T. *J. Am. Chem. Soc.* **1980**, *102*, 1740–1742.

(55) Ishino, M.; Tamura, M.; Deguchi, T.; Nakamura, S. *J. Catal.* **1992**, *133*, 332–341.

(56) Tóth, I.; Elsevier, C. J. *J. Am. Chem. Soc.* **1993**, *115*, 10388–10389.

(57) Elsevier, C. J. *J. Mol. Catal.* **1994**, *92*, 285–297.

(58) Whitbeck, M. R. Second Derivative Infrared Spectroscopy. *Appl. Spectrscopy* **1981**, *35*, 93–95.

(59) Owen, A. J. Uses of derivative spectroscopy; Publication Number 5963-3940E; Application Note for Agilent Technologies: Santa Clara, CA, 1995.

(60) Chew, W.; Widjaja, E.; Garland, M. *Organometallics* **2002**, *21*, 1982–1990.

(61) Rauhut, G.; Pulay, P. *J. Phys. Chem.* **1995**, *99*, 3093–3100.

(62) Halls, M. D.; Velkovski, J.; Schlegel, H. B. *Theor. Chem. Acc.* **2001**, *105*, 413–421.

(63) Kesharwani, M. K.; Brauer, B.; Martin, J. M. L. *J. Phys. Chem. A* **2015**, *119*, 1701–1714.

(64) Sinha, P.; Boesch, S. E.; Gu, C.; Wheeler, R. A.; Wilson, A. K. *J. Phys. Chem. A* **2004**, *108*, 9213–9217.

(65) Scott, A. P.; Radom, L. *J. Phys. Chem.* **1996**, *100*, 16502–16513.

(66) Kohls, E.; Stein, M. *Contrib. Sect. Nat. Math. Biotech. Sci.* **2017**, *38*, 43–57.

(67) Smith, R. D.; Simmons, H. E. *Org. Synth.* **1961**, *41*, 72.

(68) Wender, P. A.; Dyckman, A. J.; Husfeld, C. O.; Scanio, M. J. C. *Org. Lett.* **2000**, *2*, 1609–1611.

(69) Bondi, A. *J. Phys. Chem.* **1964**, *68*, 441–451.

(70) Rowland, R. S.; Taylor, R. *J. Phys. Chem.* **1996**, *100*, 7384–7391.

(71) Marenich, A. V; Cramer, C. J.; Truhlar, D. G. *J. Phys. Chem. B* **2009**, *113*, 6378–6396.

(72) Dauben, H. J. J.; McCoy, L. L. *J. Am. Chem. Soc.* **1959**, *81*, 4863–4873.

(73) Shao, Y.; Molnar, L. F.; Jung, Y.; Kussmann, J.; Ochsenfeld, C.; Brown, S. T.; Gilbert, A. T. B.; Slipchenko, L. V.; Levchenko, S. V.; O'Neill, D. P.; et al. *Phys. Chem. Chem. Phys.* **2006**, *8*, 3172–3191.

(74) Chai, J. Da; Head-Gordon, M. *Phys. Chem. Chem. Phys.* **2008**, *10*, 6615–6620.

(75) Stewart, J. J. P. *J. Comput. Chem.* **1989**, *10*, 209–220.

(76) Lee, C.; Yang, W.; Parr, R. G. *Phys. Rev. B* **1988**, *37*, 785–789.

(77) Becke, A. D. *J. Chem. Phys.* **1993**, *98*, 5648–5652.

(78) Benson, S. W. *The Foundations of Chemical Kinetics*; Krieger: Malabar, FL, 1982.

(79) Okuno, Y. *Chem. - Eur. J.* **1997**, *3*, 212–218.

(80) Schoenebeck, F.; Houk, K. N. *J. Am. Chem. Soc.* **2010**, *132*, 2496–2497.

(81) Xie, H.; Lin, Z. *Organometallics* **2014**, *33*, 892–897.

(82) Quesnel, J. S.; Moncho, S.; Ylijoki, K. E. O.; Torres, G.; Brothers, E. N.; Bengali, A. A.; Amdtsen, B. A. *Chem. - Eur. J.* **2016**, *22*, 15107–15118.

(83) Macrae, C. F.; Bruno, I. J.; Chisholm, J. A.; Edgington, P. R.; McCabe, P.; Pidcock, E.; Rodriguez-Monge, L.; Taylor, R.; Van De Streek, J.; Wood, P. A. *J. Appl. Crystallogr.* **2008**, *41*, 466–470.

(84) APEX II, Bruker AXS Inc.: Madison, Wisconsin, USA. 2008.

(85) SAINT, Bruker AXS Inc.: Madison, Wisconsin, USA. 2008.

(86) SADABS, Bruker AXS Inc.: Madison, Wisconsin, USA. 2009.

(87) Sheldrick, G. M. *Acta Crystallogr. Sect. A Found. Crystallogr.* **2008**, *64*, 112–122.

(88) Sheldrick, G. M. *Acta Crystallogr. Sect. A Found. Crystallogr.* **2015**, *71*, 3–8.

(89) Sheldrick, G. M. *Acta Crystallogr. Sect. C Struct. Chem.* **2015**, *71*, 3–8.

(90) Spek, A. L. *Acta Crystallogr. Sect. D Biol. Crystallogr.* **2009**, *65*, 148–155.

Chapter 6 – Appendix

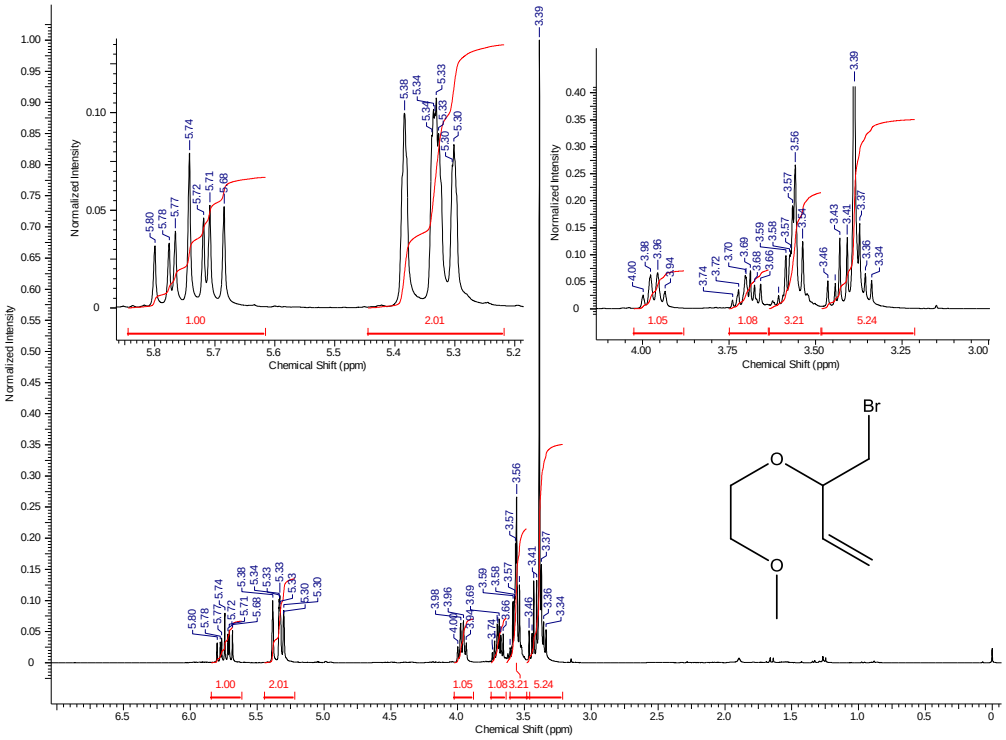

Figure A.1: ^{1}H NMR (300 MHz, $CDCl_3$) spectrum of brominated intermediate **1**.

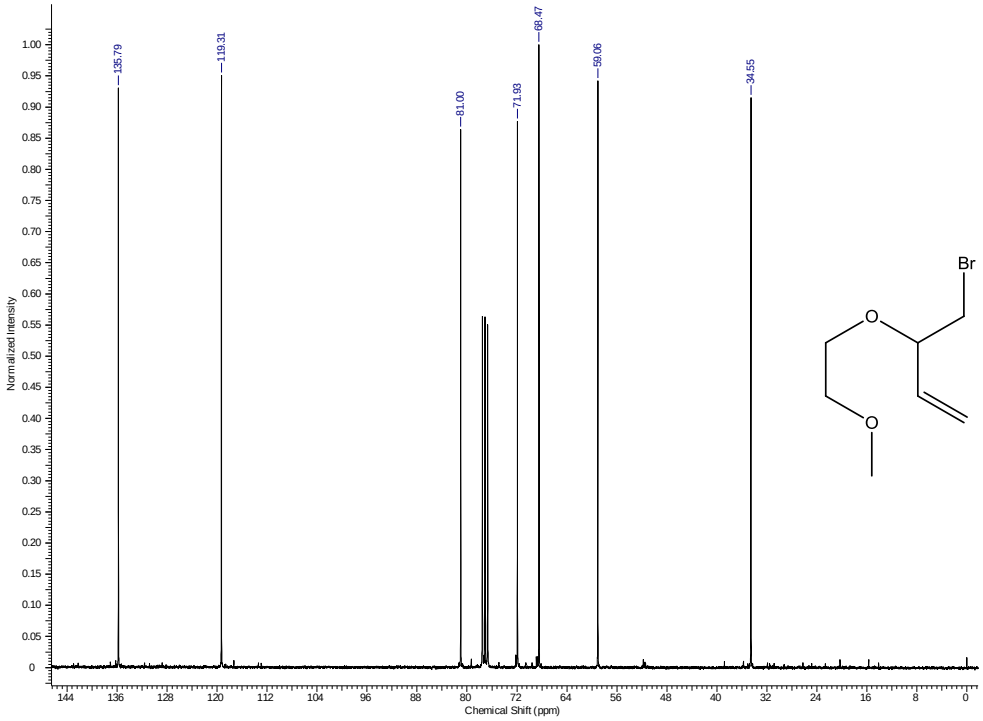

Figure A.2: $^{13}C\{^{1}H\}$ NMR (75 MHz, $CDCl_3$) spectrum of brominated intermediate **1**.

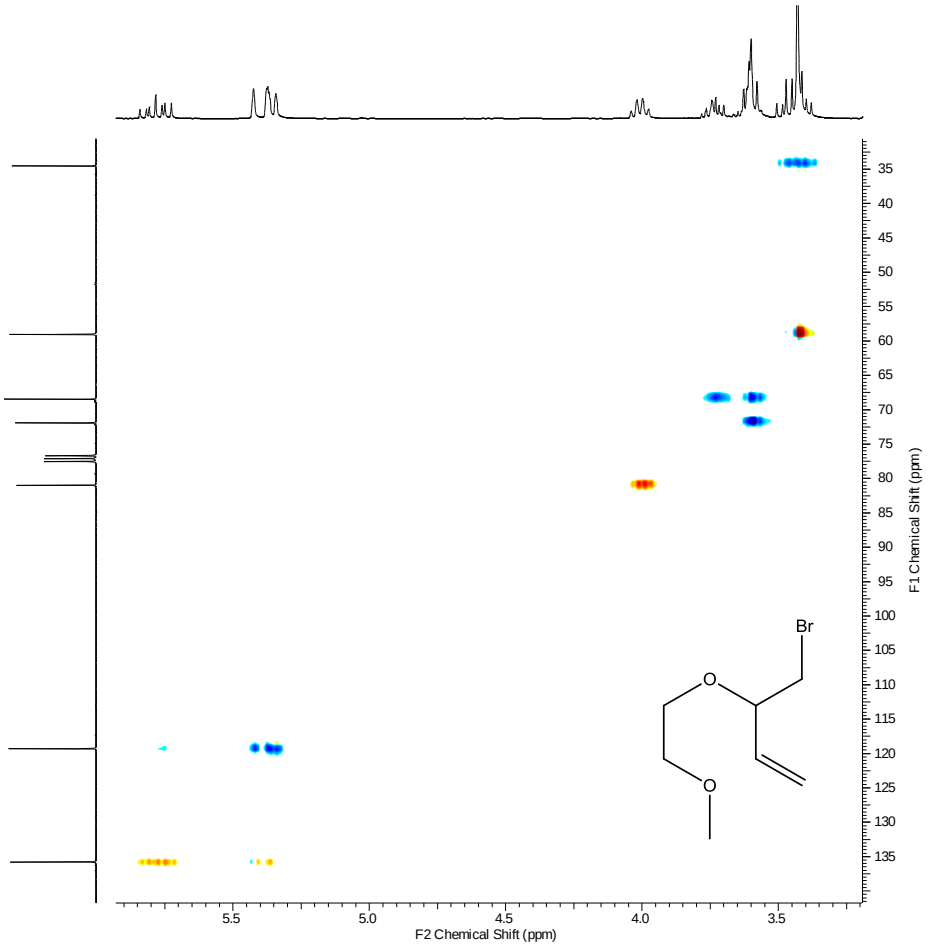

Figure A.3: HSQC (^{1}H, ^{13}C single bond correlation) spectrum of brominated intermediate **1**.

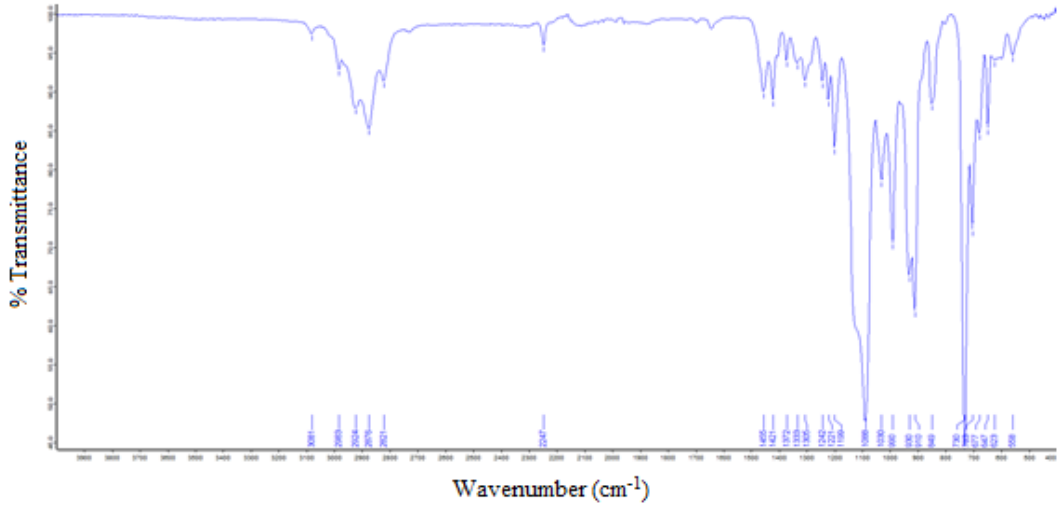

Figure A.4: ATR FTIR spectrum (neat) of brominated intermediate **1**, showing % transmittance as a function of wavenumber.

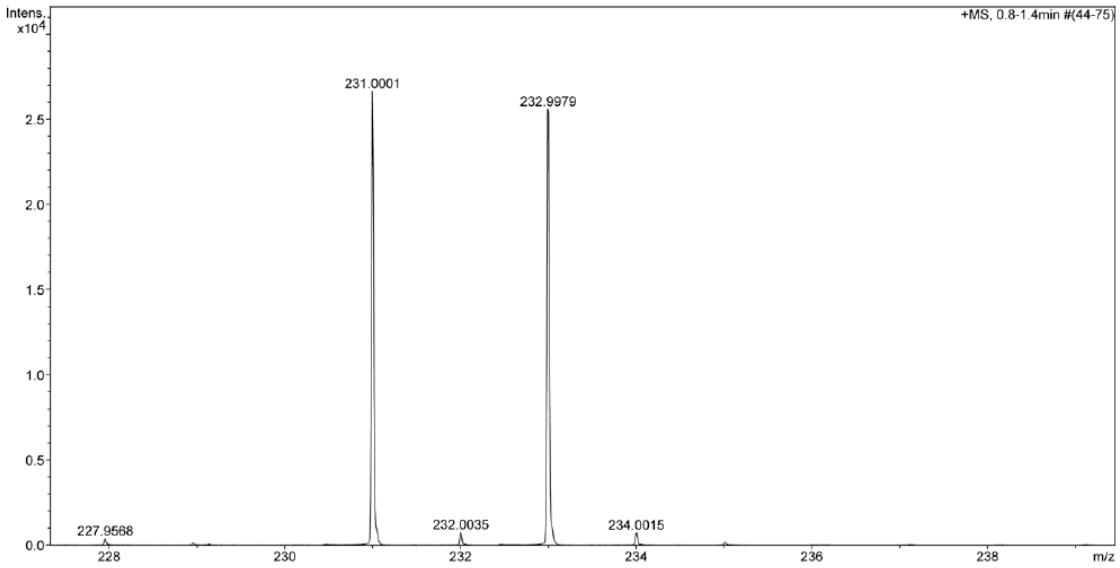

Figure A.5: HRMS spectrum of brominated intermediate **1**.

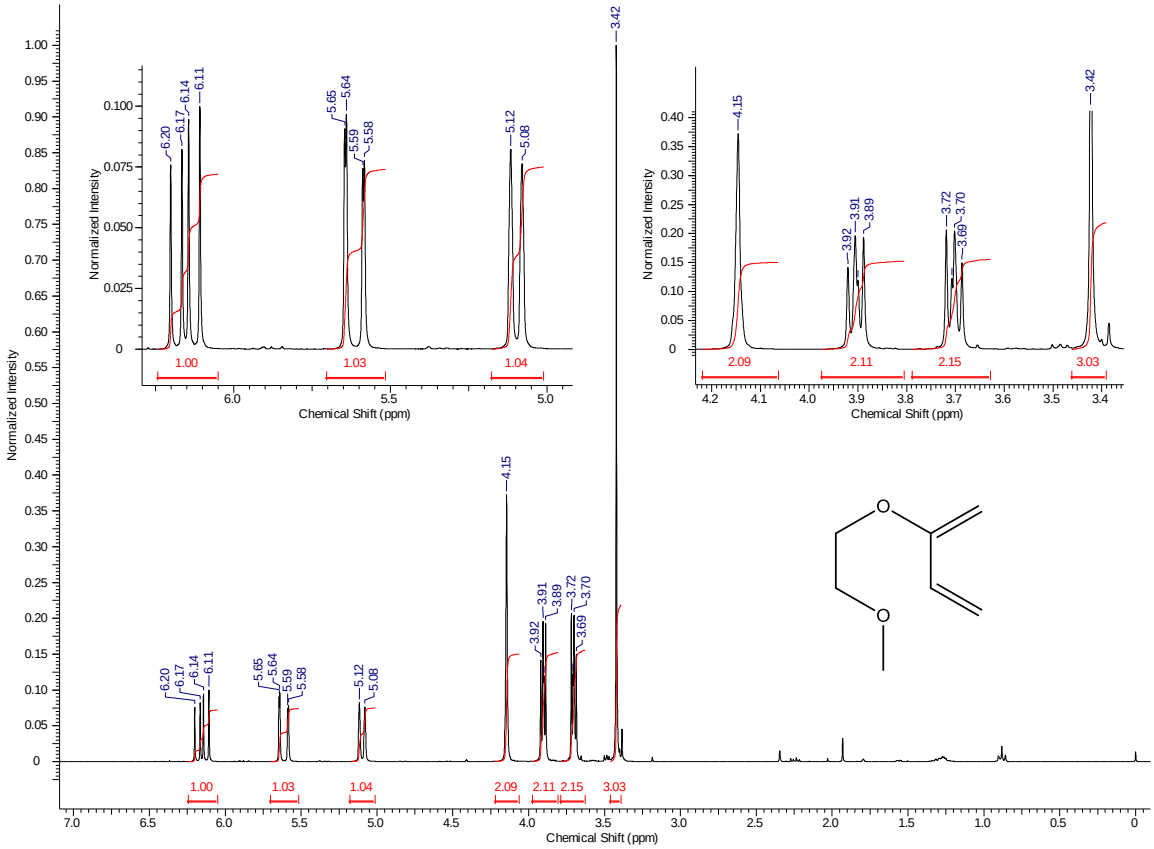

Figure A.6: ^{1}H NMR (300 MHz, $CDCl_3$) spectrum of diene **2**.

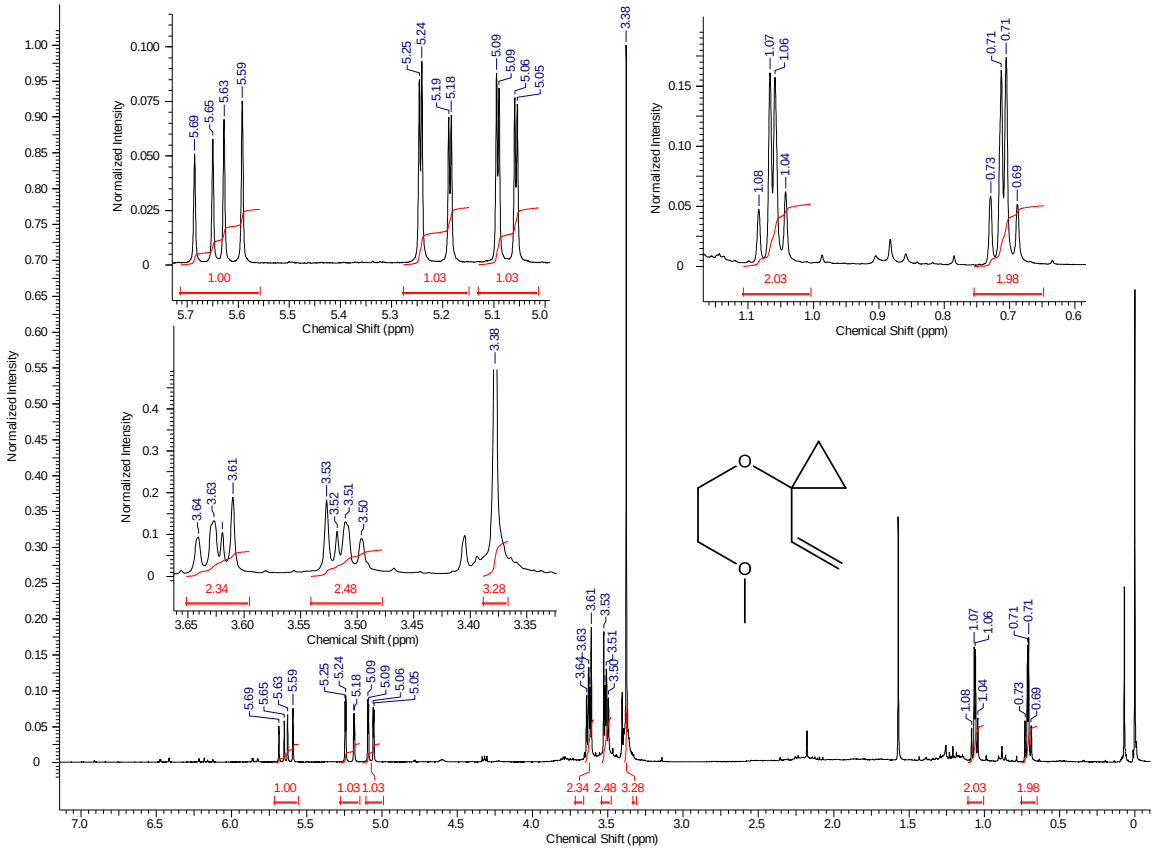

Figure A.7: ^{1}H NMR (300 MHz, $CDCl_3$) spectrum of VCP **3**.

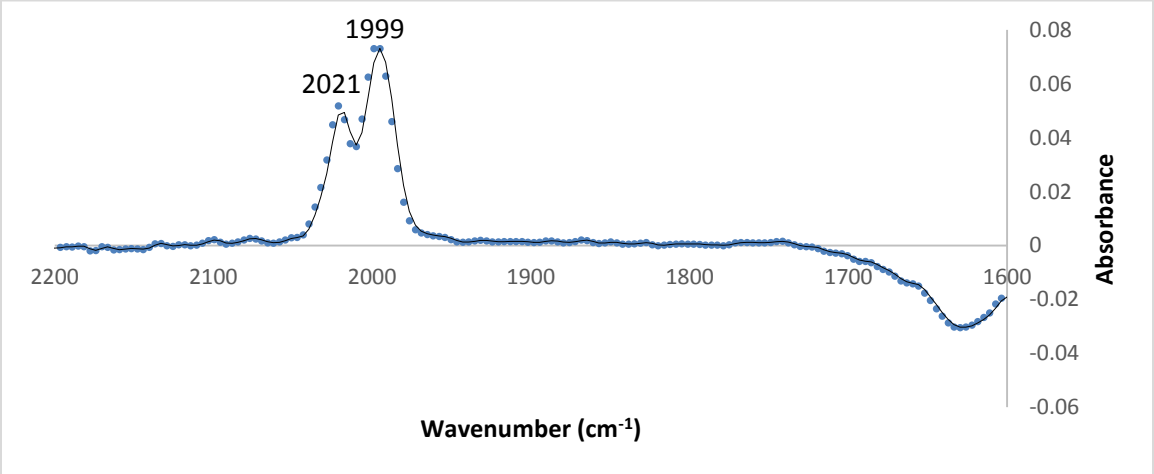

Figure A.8: IR spectrum of CO in toluene, showing absorbance as a function of wavenumber.

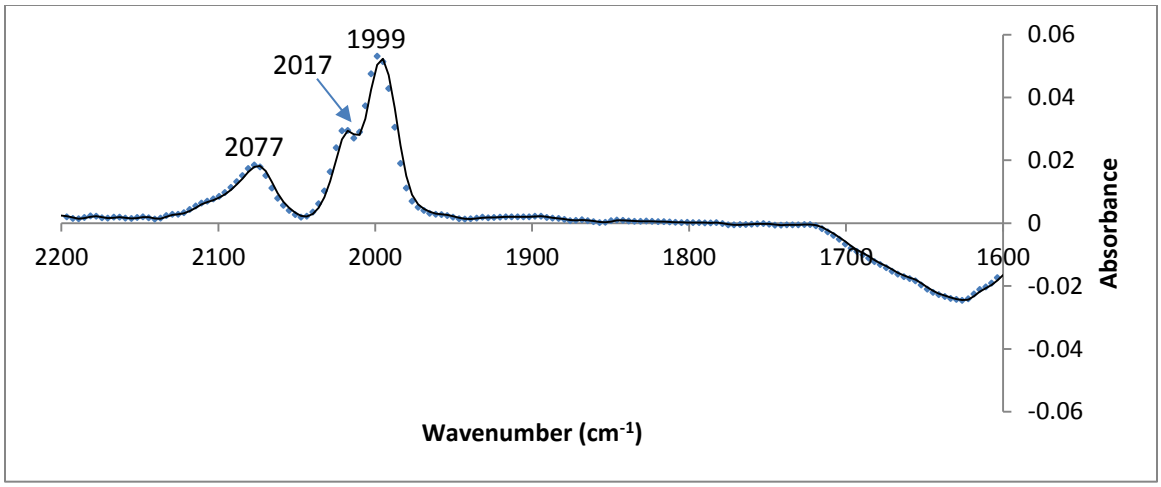

Figure A.9: IR spectrum of Rh catalyst solution (2.7 mol%) after the addition of VCP, alkyne, and CO, showing absorbance as a function of wavenumber.

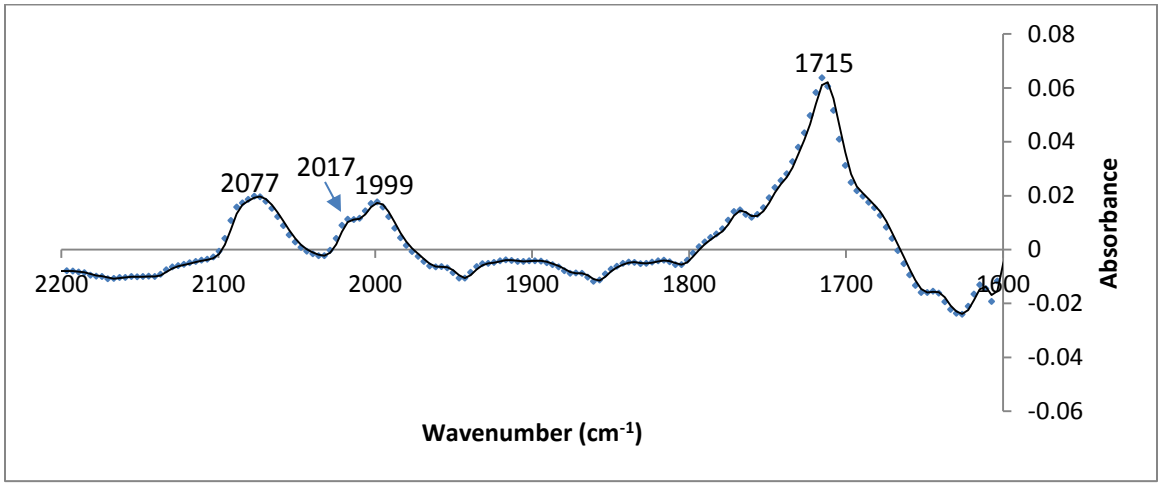

Figure A.10: IR spectrum of Rh catalyst solution (2.7 mol %) after the addition of VCP, alkyne, and CO after 35 h of heating at 60 ºC showing absorbance as a function of wavenumber.

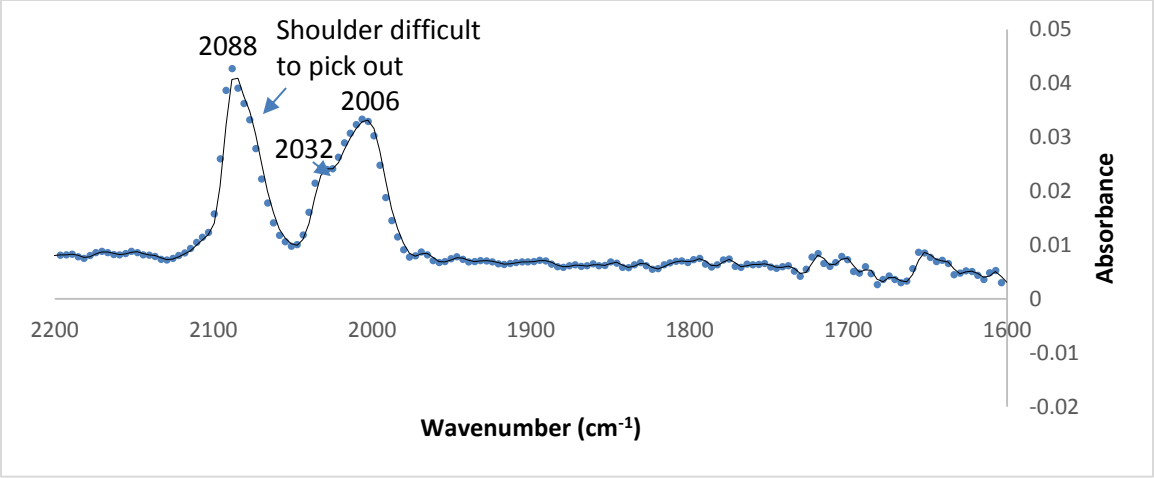

Figure A.11: IR spectrum of **BM1** showing absorbance as a function of wavenumber.

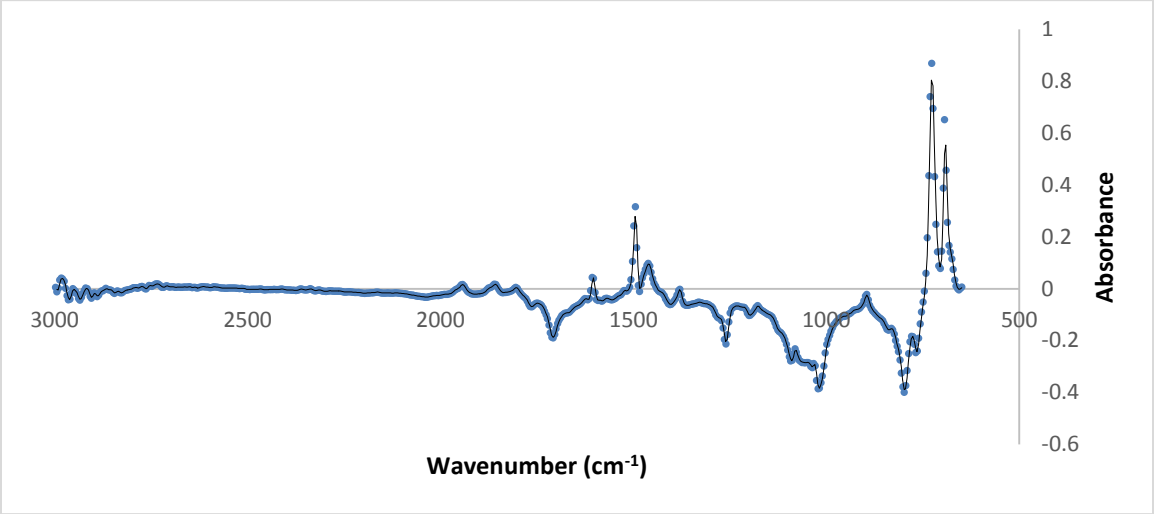

Figure A.12: IR reference spectrum of toluene showing absorbance as a function of wavenumber.

Table A.1. Crystal data and structure refinement.

Identification code	KY013	RM_KY_001	RM_KY_002
Empirical formula	C_{12} $H_{14}Cl_2O_6Rh_2$	$C_{21}H_{16}O_2$	$C_4Cl_2O_4Rh_2$
Formula weight	530.95	300.34	388.76
Temperature	125(2) K	125(2) K	125(2) K
Wavelength	0.71073 Å	0.71073 Å	0.71073 Å
Crystal system	Monoclinic	Monoclinic	Tetragonal
Space group	$P2_1/c$	$P2_1/c$	$I\text{-}42d$
Unit cell dimensions	a = 6.6800(4) Å b = 18.2800(12) Å c = 13.5307(9) Å α = 90° β = 92.1040(10)° γ = 90°	a = 9.384(3) Å b = 11.032(4) Å c = 14.827(5) Å α = 90° β = 102.609(4)° γ = 90°	a = 14.0370(15) Å b = 14.0370(15) Å c = 9.2038(10) Å α = 90° β = 90° γ = 90°
Volume	1651.13(18) $Å^3$	1498.0(9) $Å^3$	1813.5(4) $Å^3$
Z	4	4	8
Density (calculated)	2.136 Mg/m^3	1.332 Mg/m^3	2.848 Mg/m^3
Absorption coefficient	2.345 mm^{-1}	0.085 mm^{-1}	4.196 mm^{-1}
F(000)	1032	632	1440
Crystal size	0.350 x 0.100 x 0.050 mm^3	0.225 x 0.200 x 0.150 mm^3	0.400 x 0.320 x 0.200 mm^3
Theta range for data collection	1.873 to 28.803°	1.407 to 25.396°	2.646 to 28.853°
Index ranges	-9<=h<=8, -24<=k<=24, -18<=l<=17	-11<=h<=11, -13<=k<=13, -17<=l<=17	-18<=h<=18, -18<=k<=19, -11<=l<=12
Reflections collected	19574	14915	10579
Independent reflections	4097 [R(int) = 0.0367]	2745 [R(int) = 0.1166]	1161 [R(int) = 0.0194]
Completeness to theta = 25.242º	100.0 %	100.0 %	100.0 %
Absorption correction	Semi-empirical from equivalents	Semi-empirical from equivalents	Semi-empirical from equivalents
Max. and min. transmission	0.7458 and 0.6282	0.7452 and 0.5078	0.7458 and 0.6313
Refinement method	Full-matrix least-squares on F^2	Full-matrix least-squares on F^2	Full-matrix least-squares on F^2
Data / restraints / parameters	4097 / 0 / 208	2745 / 1 / 212	1161 / 0 / 55
Goodness-of-fit on F^2	1.011	1.077	1.140
Final R indices [I>2sigma(I)]	R1 = 0.0247, wR2 = 0.0455	R1 = 0.0792, wR2 = 0.2030	R1 = 0.0103, wR2 = 0.0244
R indices (all data)	R1 = 0.0377, wR2 = 0.0491	R1 = 0.1320, wR2 = 0.2334	R1 = 0.0106, wR2 = 0.0244
Extinction coefficient	n/a	n/a	n/a
Largest diff. peak and hole	0.635 and -0.528 e.$Å^{-3}$	0.371 and -0.307 e.$Å^{-3}$	0.265 and -0.220 e.$Å^{-3}$